

1 Seawater pH reconstruction using boron isotopes in multiple planktonic foraminifera species with
2 different depth habitats and their potential to constrain pH and pCO₂ gradients
3
4

5 Maxence Guillermic^{1,2}, Sambuddha Misra^{3,4}, Robert Eagle^{1,2}, Alexandra Villa^{2,5}, Fengming Chang⁶,
6 Aradhna Tripathi^{1,2}
7
8
9
10

11 ¹ Department of Earth, Planetary, and Space Sciences, Department of Atmospheric and Oceanic
12 Sciences, Institute of the Environment and Sustainability, UCLA, University of California – Los
13 Angeles, Los Angeles, CA 90095 USA

14 ² Laboratoire Géosciences Océan UMR6538, UBO, Institut Universitaire Européen de la Mer, Rue
15 Dumont d'Urville, 29280, Plouzané, France

16 ³ Indian Institute of Science, Centre for Earth Sciences, Bengaluru, Karnataka 560012, India

17 ⁴ The Godwin Laboratory for Palaeoclimate Research, Department of Earth Sciences, University of
18 Cambridge, UK

19 ⁵ Department of Geology, University of Wisconsin-Madison, Madison, WI 53706 USA

20 ⁶ Key Laboratory of Marine Geology and Environment, Institute of Oceanology, Chinese Academy of
21 Sciences, Qingdao 266071, China
22
23
24
25
26
27
28
29
30
31
32
33
34
35
36

37 Submitted to Biogeosciences
38
39
40

41 *Corresponding authors:

42 E-mail address: maxence.guillermic@gmail.com, atripati@ucla.edu
43

44 **ABSTRACT**

45

46 Boron isotope systematics of planktonic foraminifera from core-top sediments and culture experiments have been
47 studied to investigate the sensitivity of $\delta^{11}\text{B}$ of calcite tests to seawater pH. However, our knowledge of the
48 relationship between $\delta^{11}\text{B}$ and pH remains incomplete for many taxa. Thus, to expand the potential scope of
49 application of this proxy, we report $\delta^{11}\text{B}$ data for 7 different species of planktonic foraminifera from sediment
50 core-tops. We utilize a method for the measurement of small samples of foraminifera and calculate the $\delta^{11}\text{B}$ -calcite
51 sensitivity to pH for *Globigerinoides ruber*, *Trilobus sacculifer* (sacc or w/o sacc), *Orbulina universa*, *Pulleniatina*
52 *obliquiloculata*, *Neogloboquadrina dutertrei*, *Globorotalia menardii* and *Globorotalia tumida*, including for
53 unstudied core-tops and species. These taxa have diverse ecological preferences and are from sites that span a
54 range of oceanographic regimes, including some that are in regions of air-sea equilibrium and others that are out
55 of equilibrium with the atmosphere. The sensitivity of $\delta^{11}\text{B}_{\text{carbonate}}$ to $\delta^{11}\text{B}_{\text{borate}}$ (eg. $\Delta\delta^{11}\text{B}_{\text{carbonate}}/\Delta\delta^{11}\text{B}_{\text{borate}}$) in core-
56 tops is consistent with previous studies for *T. sacculifer* and *G. ruber* and close to unity for *N. dutertrei*, *O. universa*
57 and combined deep-dwelling species. Deep-dwelling species closely follow the core-top calibration for *O.*
58 *universa*, which is attributed to respiration-driven microenvironments likely caused by light limitation and/or
59 symbiont/host interactions. Our data support the premise that utilizing boron isotope measurements of multiple
60 species within a sediment core can be utilized to constrain vertical profiles of pH and pCO_2 at sites spanning
61 different oceanic regimes, thereby constraining changes in vertical pH gradients and yielding insights into the past
62 behavior of the oceanic carbon pumps.

63 1. Introduction

64 The oceans are absorbing a substantial fraction of anthropogenic carbon emissions resulting in declining
65 surface ocean pH (IPCC, 2014). Yet there is a considerable uncertainty over the magnitude of future pH change in
66 different parts of the ocean and the response of marine biogeochemical cycles to physio-chemical parameters (T,
67 pH) caused by climate change (Bijma et al., 2002; Ries et al., 2009). Therefore, there is an increased interest in
68 reconstructing past seawater pH (Hönisch and Hemming, 2004; Liu et al., 2009; Wei et al., 2009; Douville et al.,
69 2010), in understanding spatial variability in aqueous pH and carbon dioxide ($p\text{CO}_2$) (Foster et al., 2008; Martinez-
70 Boti et al., 2015b; Raitzsch et al., 2018), and in studying the response of the biological carbon pump using
71 geochemical proxies (Yu et al., 2007, 2010, 2016).

72 Although all proxies for carbon cycle reconstruction are complex in nature (Pagani et al., 2005; Tripathi et
73 al., 2009, 2011; Allen and Hönisch, 2012), the boron isotope composition of foraminiferal tests (expressed as
74 $\delta^{11}\text{B}_{\text{carbonate}}$) is emerging as one of the more robust available tools (Ni et al., 2007; Foster et al., 2008, 2012; Henehan
75 et al., 2013; Martinez-Boti et al., 2015b; Chalk et al., 2017). The study of laboratory-cultured foraminifera has
76 demonstrated a systematic dependence of the boron isotope composition of tests on solution pH (Sanyal et al.,
77 1996, 2001; Henehan et al., 2013, 2016). Core-top measurements on globally distributed samples also show a
78 boron isotope ratio sensitivity to pH with taxa-specific offsets from the theoretical fractionation line of borate ion
79 (Rae et al., 2011; Henehan et al., 2016; Raitzsch et al., 2018).

80 Knowledge of seawater pH, in conjunction with constraints on one other carbonate system parameter
81 (Total Alkalinity (TA), DIC (dissolved inorganic carbon), $[\text{HCO}_3^-]$, $[\text{CO}_3^{2-}]$), can be utilized to constrain aqueous
82 $p\text{CO}_2$. Application of empirical calibrations for boron isotope ratio, determined for select species of foraminifera
83 from core-tops and laboratory cultures, has resulted in accurate reconstructions of $p\text{CO}_2$ utilizing downcore
84 samples from sites that are currently in quasi-equilibrium with the atmosphere at present. Values of $p\text{CO}_2$
85 reconstructed from planktonic foraminifera boron isotope ratios are analytically indistinguishable from ice core
86 CO_2 records (Foster et al., 2008; Henehan et al., 2013; Chalk et al., 2017).

87 The last decade has produced several studies aiming at reconstructing past seawater pH using boron
88 isotopes to constrain atmospheric $p\text{CO}_2$ in order to understand the changes in the global carbon cycle (Hönisch et
89 al., 2005, 2009; Foster et al., 2008, 2012, 2014; Seki et al., 2010; Bartoli et al., 2011; Henehan et al., 2013;
90 Martinez-Boti et al., 2015a, 2015b; Chalk et al., 2017). In addition to reconstructing atmospheric $p\text{CO}_2$, the boron
91 isotopes proxy has been applied to mixed-layer planktonic foraminifera at sites out of equilibrium with the
92 atmosphere to constrain past air-sea fluxes (Foster et al., 2014; Martinez-Boti et al., 2015b). A small body of work
93 has examined whether data for multiple species in core-top (Foster et al., 2008) and down-core samples could be
94 used to constrain vertical profiles of pH through time (Palmer et al., 1998; Pearson and Palmer, 1999; Anagnostou
95 et al., 2016).

96 Here we add to the emerging pool of boron isotope data in planktonic foraminifera from different
97 oceanographic regimes, including data for species that have not previously been examined. We utilize a low-blank
98 (15 pg B to 65 pg B), high precision (2sd on the international standard JCP-1 is 0.20 ‰, n=6) $\delta^{11}\text{B}_{\text{carbonate}}$ analysis
99 method for small samples (down to ~250 $\mu\text{g CaCO}_3$), modified after Misra et al. (2014), to study multiple species
100 of planktonic foraminifera. The studied sediment core-tops span a range of oceanographic regimes, including open-
101 ocean oligotrophic settings and marginal seas. We constrain calibrations for different species, and compare results
102 to published work (Foster et al., 2008; Henehan et al., 2013; Henehan et al., 2016; Martinez-Boti et al., 2015b;

103 Raitzsch et al., 2018). We also test whether these data support the application of boron isotope measurements of
104 multiple species within a sediment core as a proxy for constraining vertical profiles of pH and pCO₂.

105

106 **2. Background**

107 **2.1 Planktonic foraminifera as archives of seawater pH**

108 Planktonic foraminifera are used as archives of past environmental conditions within the mixed layer and
109 thermocline, as their chemical composition is correlated with the physio-chemical parameters of their calcification
110 environment (Ravelo and Fairbanks, 1992; Elderfield and Ganssen, 2000; Dekens et al., 2002; Anand et al., 2003;
111 Sanyal et al., 2001; Ni et al., 2007; Henehan et al., 2013, 2015, 2016; Howes et al., 2017; Raitzsch et al., 2018).
112 The utilization of geochemical data for multiple planktonic foraminifera species with different ecological
113 preferences to constrain vertical gradients has been explored in several studies. The framework for such an
114 approach was first developed using modern samples of planktonic foraminifera for oxygen isotopes, where it was
115 proposed as a tool to constrain vertical temperature gradients and study physical oceanographic conditions during
116 periods of calcification (Ravelo and Fairbanks, 1992).

117 Because planktonic foraminifera species complete their lifecycle in a particular depth habitat due to their
118 ecological preference (Ravelo and Fairbanks, 1992; Farmer et al., 2007), it is theoretically possible to reconstruct
119 water column profiles of pH using boron isotope ratios data from multiple taxa (Palmer and Pearson, 1998;
120 Anagnostou et al., 2016). The potential use of an analogous approach to reconstruct past profiles of seawater pH
121 was first highlighted by Palmer and Pearson (1998) on Eocene samples to constrain pH-depth gradients. However,
122 in these boron isotope-based studies, it was assumed that boron isotope offset from seawater and foraminiferal
123 carbonate were constant, which is an assumption not supported by subsequent studies (e.g., Hönisch et al., 2003;
124 Foster et al., 2008; Henehan et al., 2013, 2016; Raitzsch et al., 2018; Rae, 2018). Furthermore, boron isotope ratio
125 differences between foraminifera species inhabiting waters of the same pH makes the acquisition of more core-
126 top and culture data essential for applications of the proxy.

127

128 **2.2 Boron systematics in seawater**

129 Boron is a conservative element in seawater with a long residence time ($\tau_B \sim 14$ Myr) (Lemarchand et al.,
130 2002a). In seawater, boron exists as trigonal boric acid B(OH)₃ and tetrahedral borate ion B(OH)₄⁻ (borate). The
131 relative abundance of boric acid and borate ion is a function of the ambient seawater pH. At standard open ocean
132 conditions (T = 25 °C and S = 35), the dissociation constant of boric acid is 8.60 (Dickson, 1990), implying that
133 boron mainly exists in the form of boric acid in seawater. Since the pK_B and seawater pH (e.g., ~8.1, NBS) values
134 are similar, it implies that small changes in seawater pH will induce strong variations in the abundance of the two
135 boron species (Fig. 1).

136 Boron has two stable isotopes, ¹⁰B and ¹¹B, with average relative abundances of 19.9 and 80.1 %, respectively. Variations in B isotope ratio are expressed in conventional delta (δ) notation:

138

$$139 \quad \delta^{11}\text{B} (\text{‰}) = 1000 \times \left(\frac{{}^{11}\text{B}/{}^{10}\text{B}_{\text{Sample}}}{{}^{11}\text{B}/{}^{10}\text{B}_{\text{NIST SRM 951}}} - 1 \right) \quad (1)$$

140

141 where positive values represent enrichment in the heavy isotope ^{11}B , and negative values enrichment in the light
142 isotope ^{10}B , relative to the standard reference material. Boron isotope values are reported versus the NIST SRM
143 951 boric acid standard (Cantazaro et al., 1970).

144 $\text{B}(\text{OH})_3$ is enriched in ^{11}B compared to $\text{B}(\text{OH})_4^-$ with a constant offset between the two chemical
145 species, within the range of physio-chemical variation observed in seawater, given by the fraction factor (α). The
146 fractionation (ϵ) between $\text{B}(\text{OH})_3$ and $\text{B}(\text{OH})_4^-$ of $27.2 \pm 0.6 \text{ ‰}$ has been empirically determined by Klochko et
147 al. (2006) in seawater. Note, Nir et al. (2015) calculate this fractionation, using an independent method, to be 26
148 $\pm 1 \text{ ‰}$, which is within the analytical uncertainty of the Klochko et al. (2006) value. We use a fractionation of 27.2
149 ‰ determined by Klochko et al. (2006) in this study.

150

151 **2.3 Boron isotopes in planktonic foraminifera calcite**

152 Many biogenic carbonate-based geochemical proxies are affected by “vital effects” or biological
153 fractionations (Urey et al., 1951). The $\delta^{11}\text{B}_{\text{carbonate}}$ in foraminifera exhibits species-specific offsets (see Rae et al.,
154 2018 for review) compared to theoretical predictions for the boron isotopic composition of $\text{B}(\text{OH})_4^-$ (expressed as
155 $\delta^{11}\text{B}_{\text{borate}}$, $\alpha=1.0272$, Klochko et al., 2006). As the analytical and technical aspects of boron isotope measurements
156 have improved (Foster et al., 2008; Rae et al., 2011; Misra et al., 2014; Lloyd et al., 2018), evidence for taxonomic
157 differences have not been eliminated, but have become increasingly apparent (Foster et al., 2008, 2018; Henehan
158 et al 2013, 2016; Foster et al., 2016; Rae et al., 2018; Raitzsch et al., 2018).

159 At present, culture and core-top calibrations have been published for several planktonic species including
160 *Trilobatus sacculifer*, *Globigerinoides ruber*, *Globigerina bulloides*, *Neogloboquadrina pachyderma*, *Orbulina*
161 *universa* (Foster et al., 2008; Henehan et al., 2013; Henehan et al., 2015; Sanyal et al., 1996; Sanyal et al., 2001).
162 Although the boron isotopic composition of several species of foraminifera is now commonly used for
163 reconstructing surface seawater pH, for other species, there is a lack of data constraining the sensitivity of boron
164 isotopes in foraminiferal carbonate and borate ion in seawater.

165

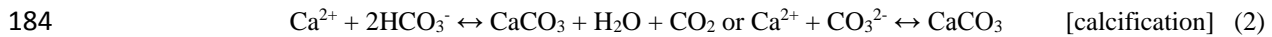
166 **2.4 Origin of biological fractionations in foraminifera**

167 Perforate foraminifera are calcifying organisms that maintain a large degree of biological control over
168 their calcification space, and thus, mechanisms of biomineralization may be of significant importance in
169 controlling the $\delta^{11}\text{B}$ of the biogenic calcite. The biomineralization of foraminifera is based on seawater
170 vacuolization (Erez, 2003; de Nooijer et al., 2014) with parcels of seawater being isolated by an organic matrix
171 thereby creating a vacuole filled with seawater. Recent work has also demonstrated that even if the chemical
172 composition of the reservoirs is modified by the organism, seawater is directly involved in the calcification process
173 with vacuoles formed at the periphery of the shell (de Nooijer et al., 2014). Culture experiments by Rollion-Bard
174 and Erez (2010) have proposed that the pH at the site of biomineralization is elevated to an upper pH limit of ~ 9
175 for the shallow-water, symbiont-bearing benthic foraminifera *Amphistegina lobifera*, which would support a pH
176 modulation of a calcifying fluid in foraminifera. The extent to which these results apply to planktonic foraminifera
177 is not known, although pH modulation of calcifying fluid may influence the $\delta^{11}\text{B}$ of planktonic foraminifera.

178 For taxa with symbionts, the microenvironment surrounding the foraminifera is chemically different from
179 seawater due to photosynthetic activity (Jorgensen et al., 1985; Rink et al., 1998; Köhler-Rink and Kühl, 2000).
180 Photosynthesis by symbionts elevates the pH of microenvironments (Jorgensen et al., 1985; Rink et al., 1998;

181 Wolf-Gladrow et al., 1999; Köhler-Rink and Kühl, 2000), while calcification and respiration decrease
182 microenvironment pH (Equation 2 and 3).

183



186

187 $\delta^{11}\text{B}$ in foraminifera is primary controlled by seawater pH, but also depends on the pH alteration of
188 microenvironments due to calcification, respiration and symbiont photosynthesis. $\delta^{11}\text{B}_{\text{carbonate}}$ should therefore
189 reflect the relative dominance of these processes and may account for species-specific $\delta^{11}\text{B}$ offsets. Theoretical
190 predictions from Zeebe et al. (2003) and foraminiferal data from Hönisch et al. (2003) explored the influence of
191 microenvironment pH in $\delta^{11}\text{B}$ signature of foraminifera. Their work also suggested that for a given species, there
192 should be a constant offset observed between the boron isotope composition of foraminifera and borate ion over a
193 large range of pH, imparting confidence in utilizing species-specific boron isotope data as a proxy for seawater
194 pH.

195 Comparison of boron isotope data for multiple planktonic foraminiferal species indicate that taxa with
196 high levels of symbiont activity such as *T. sacculifer* and *G. ruber* show higher $\delta^{11}\text{B}$ values than the $\delta^{11}\text{B}$ of ambient
197 borate (Foster et al., 2008, Henehan et al., 2013, Raitzsch et al., 2018). The sensitivities ($\Delta\delta^{11}\text{B}_{\text{carbonate}}/\Delta\delta^{11}\text{B}_{\text{borate}}$,
198 hereafter referred to as the slope) of existing calibrations suggest a different species-specific sensitivity for these
199 species compared to other taxa (Sanyal et al., 2001; Henehan et al., 2013; Henehan et al., 2015; Raitzsch et al.,
200 2018). For example, *Orbulina universa* exhibits a lower $\delta^{11}\text{B}$ than *in situ* $\delta^{11}\text{B}$ values of borate ion (Henehan et
201 al., 2016), consistent with the species living deeper in the water column characterized by reduced photosynthetic
202 activity.

203 It is possible that photosynthetic activity by symbionts might not be able to compensate for changes in
204 calcification and/or respiration, leading to an acidification of the microenvironment. It is interesting to note that
205 for *O. universa* the slope determined for the field-collected samples is not statistically different from unity ($0.95 \pm$
206 0.17) (Henehan et al. 2016), while culture experiments report slopes of ≤ 1 for multiple species including *G. ruber*
207 (Henehan et al., 2013), *T. sacculifer* (Sanyal et al., 2001), and *O. universa* (Sanyal et al., 1999). More core-top and
208 culture calibrations are needed to refine those slopes and understand if significant differences are observed, which
209 is part of the motivation for this study.

210

211 **2.5 Planktic foraminifera depth and habitat preferences**

212 The preferred depth habitat of different species of planktonic foraminifera depends on their ecology,
213 which in turn is dependent on hydrographic conditions. For example, *G. ruber* is commonly found in the mixed
214 layer (Fairbanks and Wiebe, 1980; Dekens et al., 2002; Farmer et al., 2007) during the summer (Deuser et al.,
215 1981) whereas *T. sacculifer* is present in the mixed layer until mid-thermocline depths (Farmer et al., 2007) during
216 spring and summer (Deuser et al., 1981, 1989). Specimens of *P. obliquiloculata* and *N. dutertrei* are abundant
217 during winter months (Deuser et al., 1989), with an acme in the mixed layer (~60m) for *P. obliquiloculata* and at
218 mid-thermocline depths for *N. dutertrei* (Farmer et al., 2007). In contrast, *O. universa* tends to record annual
219 average conditions within the mixed layer. Specimens of *G. menardii* calcify within the seasonal thermocline
220 (Fairbanks et al., 1982, Farmer et al., 2007, Regenberg et al., 2009), and in some regions in the upper thermocline

221 (Farmer et al., 2007), and records annual temperatures. *G. tumida* is found at the lower thermocline or below the
222 thermocline and records annual average conditions (Fairbanks and Wiebe, 1980; Farmer et al., 2007, Birch et al.,
223 2013). Although the studies listed above showed evidence for species-specific living depth-habitat affinities, recent
224 direct observations showed that environmental conditions (e.g. temperature, light) was locally responsible for the
225 variability in the living depth of certain foraminifera species in the eastern North Atlantic (Rebotim et al., 2017).

226

227 3. Materials and Methods

228

229 3.1 Localities studied

230 Core-top locations were selected to span a broad range of seawater pH, carbonate system parameters, and
231 oceanic regimes. Samples from Atlantic Ocean (CD107-A), Indian Ocean (FC-01a and FC-02a), Arabian Sea
232 (FC-13a and FC-12b) and Pacific Ocean (WP07-01, A14, and Ocean Drilling Program 806A and 807A) were
233 analyzed; characteristics of the sites are summarized in Table 1 and S7, Fig. 2, and Fig. 3.

234 Atlantic site CD107-a (CD107 site A) was cored in 1997 by the Benthic Boundary Layer program
235 (BENBO) (K.S. Black et al., 1997 - cruise report RRS Charles Darwin Cruise 107). Arabian Sea sites FC-12b
236 (CD145 A150) and FC-13a (CD145 A3200) were retrieved by the *Charles Darwin* in the Pakistan Margin in 2004
237 (B.J. Bett et al., 2003 - cruise report n°50 RRS Charles Darwin Cruise 145). A14 was recovered by box corer in
238 the southern area of the South China Sea in 2012. Core WP07-01 was obtained from the Ontong Java Plateau using
239 a giant piston corer during the Warm Pool Subject Cruise in 1993. Holes 806A and 807A were retrieved on Leg
240 130 by the Ocean Drilling Program (ODP). The top 10 cm of sediment from CD107-A have been radiocarbon
241 dated to be Holocene <3 ky (Thomson et al., 2000). Samples from multiple box cores from Indian Ocean sites
242 were radiocarbon dated as Holocene <7.3 ky (Wilson et al., 2012). Samples from western equatorial Pacific Site
243 806B, close to site WP07-01, are dated to between 7.3-8.6 ky (Lea et al., 2000). Arabian Sea and Pacific core-top
244 samples were not radiocarbon dated but are assumed to be Holocene.

245

246 3.2 Species

247 Around 50-100 foraminifera shells were picked from the 400-500 µm fraction size for *Globorotalia*
248 *menardii* and *Globorotalia tumida*, >500 µm for *Orbulina universa*, and from the 250-400 µm fraction size for
249 *Trilobatus sacculifer* (w/o sacc, without sacc-like final chamber), *Trilobatus sacculifer* (sacc, sacc-like final
250 chamber), *Globigerinoides ruber* (white, sensu stricto), *Neogloboquadrina dutertrei*, and *Pulleniatina*
251 *obliquiloculata*. The samples picked for analyses were visually well preserved.

252

253 3.3 Sample cleaning

254 Briefly, picked foraminifera were gently cracked open, clay removed with successive ultrasonication
255 steps in MQ water and methanol and then were checked for coarse-grained silicates. The next stages of sample
256 processing and chemical separation were performed in a class 1000 clean lab equipped with boron-free HEPA
257 filters. Samples were cleaned using full reductive and oxidative cleaning (Boyle, 1981; Boyle and Keigwin, 1985;
258 Barker et al., 2003). Samples from the South China Sea (sites A14, E035) presented high Mn and high Fe. Due to
259 potential Fe-Mn oxide and hydroxides the reductive cleaning was used. Previous comparisons of cleaning methods
260 have shown there is no impact of the reductive step on B/Ca (Misra et al., 2014b) but there is an impact of the
261 reductive step on Mg/Ca (Barker et al., 2003 and others), nevertheless, it is possible that Fe-Mn oxide and

262 hydroxides can result in non-negligible Mg and B contamination. Because this study was designed to investigate
263 boron proxies and in order to be consistent in methodology, the reductive cleaning was used at all sites. Cleaned
264 samples selected for this study did not yield high Mn concentrations (see supplement for discussion on
265 contamination).

266 A final leaching step with 0.001N HCl was done before dissolution in 1N HCl. Hydrochloric acid was
267 used to allow complete dissolution of the sample including Fe-Mn oxide and hydroxides if present. Each sample
268 was divided into two aliquots: an aliquot for boron purification and one aliquot for trace element analysis.

269

270 3.4 Reagents

271 Double-distilled HNO₃ and HCl acids (from Merck® grade) and a commercial bottle of HF Ultrapure
272 grade were used at Brest. Double-distilled acids were used at Cambridge. All acids and further dilutions were
273 prepared using double-distilled 18.2 MΩ.cm⁻¹ MQ water. Working standards for isotope ratio and trace element
274 measurements were freshly diluted on a daily basis with the same acids used for sample preparation to avoid any
275 matrix effects.

276

277 3.5 Boron isotopes

278 Boron purification for isotopic measurement was done utilizing microdistillation method developed by
279 Gaillardet et al. (2001), for Ca-rich matrices by Wang et al. (2010) and adapted at Cambridge by Misra et al.
280 (2014a). 70 μL of carbonate sample dissolved in 1N HCl was loaded on a cap of a clean fin legged 5 mL conical
281 beaker upside down. The tightly closed beaker was put on a hotplate at 95°C for 15 hours. The beakers were taken
282 off the hotplate and were allowed to cool for 15 min. The cap where the residue formed was replaced by a clean
283 one. Then, 100 μL of 0.5% HF were added to the distillate.

284 Boron isotopic measurements were carried out on a Thermo Scientific ®Neptune+ MC-ICP-MS at the
285 University of Cambridge. Neptune+ was equipped with Jet interface and two 10¹³ Ω resistors. The instrumental
286 setup included Savillex® 50μl/min C-flow self-aspirating nebulizer, single pass Teflon® Scott-type spray chamber
287 constructed utilizing Savillex® column components, 2.0 mm Pt injector from ESI®, Thermo® Ni ‘normal’ type
288 sample cone and ‘X’ type skimmer cones. Both isotopes of boron were determined utilizing 10¹³ Ω resistors (Misra
289 et al., 2014a; Lloyd et al., 2018).

290 The sample size for boron isotope analyses typically ranged from 10 ppb B (~5 ng B) to 20 ppb B samples
291 (~10 ng B). Instrumental sensitivity for ¹¹B was 17 mV/ppb B (eg. 170 mV for 10ppb B) in wet plasma at 50μl/min
292 sample aspiration rate. Intensity of ¹¹B for a sample at 10ppb B was typically 165mV ± 5mV, which closely
293 matched the 170mV ± 5mV of the standard. Due to the low boron content of the samples extreme care was taken
294 to avoid boron contamination during sample preparation and reduce memory effect during analysis. Procedural
295 boron blanks ranged from 15pg B to 65 pg B and contributed to less than <1% of the sample signal. The acid blank
296 during analyses was measured at ≤ 1mV on ¹¹B, meaning a contribution < 1% of the sample intensity, no memory
297 effect was observed within and across sessions. No matrix effect resulting from the mix HCl/HF was observed on
298 the δ¹¹B.

299 Analyses of external standards were done to ensure data quality. For δ¹¹B measurements one carbonate
300 standard and one coral were utilized: the JcP-1 (Geological Survey of Japan, Tsukuba, Japan) international
301 standard (Gutjahr et al., 2014) and the NEP coral (Porites sp., δ¹¹B = 26.12 ± 0.92 ‰, 2SD, n=33 Holcomb et al.,

2015 and Sutton et al., 2018, Table S2) from University of Western Australia/Australian National University. A certified boric acid standard, the ERM[®] AE121 ($\delta^{11}\text{B} = 19.9 \pm 0.6 \text{ ‰}$, SD, certified) was used to monitor reproducibility and drift during each session (Vogl and Rosner, 2011; Foster et al., 2013; Misra et al., 2014). Results for the isotopic composition of the NEP coral are shown in Table S2, average values are $\delta^{11}\text{B}_{\text{NEP}} = 25.70 \pm 0.93 \text{ ‰}$ (2SD, n=22) over different 7 analytical sessions with each number representing an ab-initio processed sample. Our results are within error of published values of $26.20 \pm 0.88 \text{ ‰}$ (2SD, n = 27) and $25.80 \pm 0.89 \text{ ‰}$ (2SD, n = 6) by Holcomb et al. (2015) and Sutton et al. (2018) respectively. Chemically cleaned JCp-1 samples were measured at 24.06 ± 0.20 (2SD, n=6) and is within error of published values of $24.37 \pm 0.32 \text{ ‰}$, $24.11 \pm 0.43 \text{ ‰}$ and $24.42 \pm 0.28 \text{ ‰}$ by Holcomb et al. (2015), Farmer et al. (2016) and Sutton et al. (2018) respectively.

311

312 3.6 Trace elements

313 The calcium concentration of each sample was measured on an ICP-AES [®] Ultima 2 HORIBA at the
314 Pôle spectrometrie Océan (PSO), UMR6538 (Plouzané, France). Samples were then diluted to fixed calcium
315 concentrations (typically 10 ppm or 30 ppm Ca) using 0.1 M HNO₃ & 0.3 M HF matching multi-element standards
316 Ca concentration to avoid any matrix effects (Misra et al., 2014b). Levels of remaining HCl (<1%) in these diluted
317 samples were negligible and did not contribute to matrix effects. Trace elements (e.g. X/Ca ratios) were analyzed
318 on a Thermo Scientific [®] Element XR HR-ICP-MS at the PSO, Ifremer (Plouzané, France).

319 Trace element analyses were done at a Ca concentration of 10 or 30 ppm. The typical blanks for a 30 ppm
320 Ca session were: ⁷Li < 2%, ¹¹B < 7%, ²⁵Mg < 0.2% and ⁴³Ca < 0.02%. Additionally, blanks for a 10 ppm Ca session
321 were: ⁷Li < 2.5%, ¹¹B < 10%, ²⁵Mg < 0.4% and ⁴³Ca < 0.05%. Due to strong memory effect for boron and
322 instrumental drift on the Element XR, long sessions of conditioning were done prior analyses. Boron blanks were
323 driven below 5% of signal intensity usually after 4 to 5 days of continuous analyses of carbonate samples. External
324 reproducibility was determined on the consistency standard Cam-Wuellestorf (courtesy of the University of
325 Cambridge) (Misra et al., 2014b), Table S3. Our X/Ca ratio measurements on the external standard Cam-
326 Wuellestorf were all the time within error of the published value (Table S3) validating the robustness of our trace
327 elements data. Analytical uncertainty of a single measurement was calculated from the reproducibility of the Cam-
328 Wuellestorf, measured during a particular mass spectrometry session. The analytical uncertainties (2SD, n=31,
329 Table S3) on the X/Ca ratios are: $\pm 0.4 \mu\text{mol/mol}$ for Li/Ca, $\pm 7 \mu\text{mol/mol}$ for B/Ca and $\pm 0.01 \text{ mmol/mol}$ for Mg/Ca
330 respectively.

331

332 3.7 Oxygen isotopes

333 Carbonate $\delta^{13}\text{C}$ and $\delta^{18}\text{O}$ were measured on a Gas Bench II coupled to a Delta V mass spectrometer at the
334 stable isotope facility of Pôle spectrometrie Océan (PSO), Plouzané. Around 20 shells were weighed, crushed and
335 clay removed following the same method described in section 3.3 (Barker et al., 2003). The recovered foraminifera
336 were weighed in tubes and flushed with He gas. Samples were then digested in phosphoric acid and analyzed.
337 Results were calibrated to the VPDB scale by international standard NBS19 and analytical precision on the in-
338 house standard Ca21 was better than $\pm 0.11 \text{ ‰}$ for $\delta^{18}\text{O}$ (1SD, n=5) and $\pm 0.03 \text{ ‰}$ for $\delta^{13}\text{C}$ (1SD, n=5).

339

340 3.8 Calcification depth determination

341 We utilized two different chemo-stratigraphic methods to estimate the calcification depth (CD) in this
342 study (Table S6 and S7). The first method (CD1), commonly used in paleoceanography, utilizes $\delta^{18}\text{O}$
343 measurements of the carbonate ($\delta^{18}\text{O}_c$) to estimate calcification depths (referred to as $\delta^{18}\text{O}$ -based calcification
344 depths) (Schmidt et al., 2002; Mortyn et al., 2003; Sime et al., 2005; Farmer et al., 2007; Birsh et al., 2013).
345 Rebotim et al. (2017) also showed good correspondence between living depth habitat and calcification depth
346 derived using CD1. The second method (CD2) utilizes Mg/Ca-based temperature estimates ($T_{\text{Mg/Ca}}$) to constrain
347 calcification depths (Quintana Krupinski et al., 2017). However, we note that reductive cleaning leads to a decrease
348 in Mg/Ca that in turn would result in a bias towards deeper calcification depths, which is not the case when we
349 utilize non-Mg/Ca-based methodologies. In both cases, the prerequisite was that vertical profiles of seawater
350 temperature are available for different seasons in ocean atlases and cruise reports, and that hydrographic data and
351 geochemical proxy signatures can be compared to assess the depth in the water column that represents the taxon's
352 maximum abundance.

353 Because both methods have their uncertainties (in one case, use of taxon-specific calibrations, and in the
354 other, analytical limitations), both estimates of calcification depth were compared to published values for the basin
355 (CD3), and where available, for the same site (Table S6). To select which calcification depth to use for further
356 calculations, we first looked at CD₁, CD₂ and CD₃. If, CD₁ and CD₂ were similar we selected this calcification
357 depth, if CD₁ and CD₂ were different we chose literature values, CD₃, when available. For some less studied
358 species, like *G. tumida*, *G. menardii* or *P. obliquiloculata*, CD₃ was not always available but when available
359 showed good correspondence with our CD₂, moreover due to availability of Mg/Ca-temperature taxon-specific
360 calibrations we preferentially use CD₂ for those species.

361 We applied (based on uncertainties of our measurements) an uncertainty of $\pm 10\text{m}$ for calcification depths
362 $> 70\text{ m}$ and an uncertainty of $\pm 20\text{ m}$ when calcification depths $< 70\text{ m}$. Direct observations of living depths of
363 foraminifera remain limited. However, the depth uncertainties reported here are in line with the uncertainties
364 calculated based on direct observations in the eastern North Atlantic which give a standard error on average living
365 depths ranging from 6-22 m for the same species (Rebotim et al., 2017). The decrease in Mg/Ca due to reductive
366 cleaning was not taking into account, because it has not been studied for most of the species used in this study and
367 because the depth uncertainty applied based on $\delta^{18}\text{O}$ analytical error is conservative relative to the uncertainty of
368 a 10% decrease in Mg/Ca equivalent that would be equivalent to $\sim 1.2^\circ\text{C}$. The depth habitats utilized to derive *in*
369 *situ* parameters are summarized in Table S7.

370

371 3.9 $\delta^{11}\text{B}_{\text{borate}}$

372 Two carbonate system parameters are needed to fully constrain the carbonate system. Following the
373 approach of Foster et al., (2008) we used the GLODAP database (Key et al., 2004) corrected for anthropogenic
374 inputs in order to estimate pre-industrial carbonate system parameters at each site. Temperature, salinity and
375 pressure for each site are from the World Ocean Database 2013 (Boyer et al., 2013). We utilized the R[®] code in
376 Henehan et al, (2016) (courtesy of Michael Henehan) to calculate the $\delta^{11}\text{B}_{\text{borate}}$, $\delta^{11}\text{B}_{\text{borate}}$ uncertainty and derive
377 our calibrations. Uncertainty for $\delta^{11}\text{B}_{\text{borate}}$ utilizing Henehan's code was similar to uncertainty calculated by
378 applying 2 standard deviations of the $\delta^{11}\text{B}_{\text{borate}}$ profiles within the limits imposed by our calcification depth.

379 The Matlab[®] template provided by Zeebe and Wolf-Gladow, (2001) was used to calculate pCO₂ from
380 TA; temperature, salinity and pressure were included in the calculations. Total boron was calculated from Lee et
381 al., (2010), K₁ and K₂ were calculated from Mehrbach et al. (1973) refitted by Dickson and Millero (1987).

382 Statistical tests were made utilizing GraphPad[®] software, linear regressions for calibration where derived
383 utilizing R[®] code in Henehan et al, (2016) (courtesy of Michael Henehan) with k (number of wild bootstrap
384 replicates) equal to 500.

385

386 4. Results

387

388 4.1 Depth habitat

389 The calcification depths utilized in this paper are summarized in Tables S6 and S7, including a comparison
390 of calcification depth determination methods. The calculated calcification depths are consistent with the ecology
391 of each species and the physical properties of the water column of the sites. Specimens of *G. ruber* and *T. sacculifer*
392 appear to be living in the shallow mixed layer (0-100 m), with *T. sacculifer* living or migrating deeper than *G.*
393 *ruber* (down to 125 m). Specimens of *O. universa* and *P. obliquiloculata* are living in the upper thermocline; *G.*
394 *menardii* is found in the upper thermocline until the thermocline depth specific to the location; *N. dutertrei* is living
395 near thermocline depths and *G. tumida* is found in the lower thermocline.

396 Data from the multiple approaches for calculating calcification depth (CD1, CD2 and CD3) implies that
397 some species inhabit deeper environments in the Western Equatorial Pacific (WEP) relative to the Arabian Sea,
398 which in turn are deeper-dwelling than the same morpho-species occurring in the Indian Ocean. In some cases, we
399 find evidence for differences in habitat depth of up to ~100m between the WEP and the Arabian Sea. This trend is
400 observed for *G. ruber* and *T. sacculifer*, but not for *O. universa*.

401 Some differences are observed between the two methods for calcification depth determination that are
402 based on $\delta^{18}\text{O}$ and Mg/Ca (CD1 and CD2, respectively). These differences might be due to the choice of
403 calibration. Alternatively, our uncertainties for $\delta^{18}\text{O}$ implies larger uncertainties on calcification depth
404 determinations that use this approach, compared to Mg/Ca based estimates.

405

406 4.2 Empirical calibrations of foraminiferal $\delta^{11}\text{B}_{\text{carbonate}}$ to $\delta^{11}\text{B}_{\text{borate}}$

407 Results for the different species analyzed in this study are presented in Fig. 4, Fig. 5 and summarized in
408 Table 2; additionally, published calibrations for comparison are summarized in Table 3.

409

410 4.2.1 *G. ruber*

411 Samples were picked from the 250-300 μm fraction, except for the WEP sites where *G. ruber* shells were
412 picked from the 250-400 μm fraction. Weight per shell averaged $11 \pm 4 \mu\text{g}$ (n=4, SD) although the weight was not
413 measured on the same sub-sample analyzed for $\delta^{11}\text{B}$ and trace elements or at the WEP sites. In comparison to
414 literature, the size fraction used for this study was smaller: Foster et al. (2008) used the 300-355 μm fraction,
415 Henehan et al. (2013) utilized multiple size fractions (250-300, 250-355, 300-355, 355-400 and 400-455 μm) and
416 Raitzsch et al. (2018) used the 315-355 μm fraction.

417 Our results for *G. ruber* (Fig. 4) are in close agreement with published data from other core-tops, sediment
418 traps, tows, and culture experiments for $\delta^{11}\text{B}_{\text{borate}} > 19 \text{‰}$ (Foster et al., 2008, Henehan et al., 2013, Raitzsch et al.,

419 2018). However, the two datapoints from $\delta^{11}\text{B}_{\text{borate}} < 19 \text{ ‰}$ are lower compared to previous studies. Elevated
420 $\delta^{11}\text{B}_{\text{carbonate}}$ values relative to $\delta^{11}\text{B}_{\text{borate}}$ has been explained by the high photosynthetic activity of symbionts
421 (Hönisch et al., 2003; Zeebe et al., 2003). Three calibrations have been derived (Table 3). Linear regression on our
422 data alone yields a slope of $1.12 (\pm 1.67)$. The uncertainty is significant given limited data in our study, and given
423 this large uncertainty, our sensitivity of $\delta^{11}\text{B}_{\text{carbonate}}$ to $\delta^{11}\text{B}_{\text{borate}}$ is also consistent with the low sensitivity trend of
424 culture experiments from Sanyal et al. (2001) or Henehan et al. (2013). The second calibration made compiling all
425 data from literature shows a sensitivity similar (e.g. $0.46 (\pm 0.34)$) to the one recently published by Raitzsch et al.,
426 (2018) (e.g. $0.45 (\pm 0.16)$, Table 3). The third linear regression made only on data from the 250-400 μm fraction
427 from our study and from the 250-300 μm from Henehan et al. (2013) yields a sensitivity of $0.58 (\pm 0.91)$ similar to
428 culture experiments from Henehan et al., (2013) (e.g. $0.6 (\pm 0.16)$, Table 3). This third calibration is offset by \sim
429 0.4 ‰ ($p > 0.05$) compared to culture calibration from Henehan et al. (2013).

430

431 **4.2.2 *T. sacculifer***

432 $\delta^{11}\text{B}_{\text{carbonate}}$ results for *T. sacculifer* (sacc and w/o sacc) (Fig. 4) are compared to published data (Foster et
433 al., 2008; Martinez-Boti et al., 2015b, Raitzsch et al., 2018). Results for *T. sacculifer* are in good agreement with
434 the literature and exhibit higher $\delta^{11}\text{B}_{\text{carbonate}}$ compared to expected $\delta^{11}\text{B}_{\text{borate}}$ at their collection location. A linear
435 regression through our data alone yields a slope of 1.3 ± 0.2 but is not statistically different to the results from
436 Martinez-Boti et al. (2015b) (Table 3), ($p > 0.05$). However, when compiled with published data using the bootstrap
437 method a slope of 0.83 ± 0.48 is calculated, with a large uncertainty given the variability in the data. It is also
438 noticeable that *T. sacculifer* (w/o sacc) samples from the WEP have a $\delta^{11}\text{B}_{\text{carbonate}}$ close to expected $\delta^{11}\text{B}_{\text{borate}}$ and
439 are significantly lower compared to the combined *T. sacculifer* of other sites ($p = 0.01$, unpaired t-test). When
440 regressing data from the 250-400 μm fraction, our results are not significantly different from the regression through
441 data that combine all size fractions (Fig. 4).

442

443 **4.2.3 *O. universa* and deeper-dwelling species: *N. dutertrei*, *P. obliquiloculata*, *G. menardii* and *G. tumida***

444 Our results for *O. universa* (Fig. 4), *N. dutertrei*, *P. obliquiloculata*, *G. menardii* and *G. tumida* (Fig. 5)
445 exhibit lower $\delta^{11}\text{B}_{\text{carbonate}}$ compared to the expected $\delta^{11}\text{B}_{\text{borate}}$ at their collection location. These data for *O. universa*
446 are not statistically different from the Henehan et al. (2016) calibration ($p > 0.05$). Our results for *N. dutertrei*
447 expand upon the initial measurements presented in Foster et al. (2008). The different environments experienced
448 by *N. dutertrei* in our study permit us to extend the range and derive a calibration for this species; the slope is close
449 to unity (0.93 ± 0.55), and is not significantly different ($p > 0.05$) from the *O. universa* calibration previously
450 reported by Henehan et al. (2016) (e.g. 0.95 ± 0.17). The data for *P. obliquiloculata* exhibits the largest offset from
451 the theoretical line. The range of $\delta^{11}\text{B}_{\text{borate}}$ from the samples we have of *G. menardii* and *G. tumida* is not sufficient
452 to derive calibrations, but the $\delta^{11}\text{B}_{\text{carbonate}}$ measured for those species are in good agreement with the *N. dutertrei*
453 calibration and Henehan et al. (2016) calibration for *O. universa*.

454 For *O. universa* and all deep-dwelling species, the slopes are not statistically different from Henehan et
455 al. (2016) ($p > 0.05$) and are close to unity. If data for deep-dwelling foraminiferal species are pooled together with
456 each other and with data from Henehan et al. (2016) and Raitzsch et al. (2018), we calculate a slope of $0.95 (\pm 0.13)$
457 ($R^2 = 0.7987$, $p < 0.0001$); if only our data are used, we calculate a slope that is not significantly different ($0.82 \pm$
458 0.27 ; $p < 0.05$).

459

460 4.2.4 Comparison of core-top and culture data

461 The data for *G. ruber* and *T. sacculifer* from the core-tops we measured are broadly consistent with
462 previous published results. The calibrations between these core-top derived estimates and culture experiments are
463 not statistically different due to small datasets and uncertainties on the linear regressions (Henehan et al., 2013;
464 Marinez-Boti et al., 2015; Raitzsch et al., 2018; Table 3). The sensitivities of the species analyzed are not
465 statistically different and are close to unity.

466

467 4.3 B/Ca ratios

468 B/Ca ratios are presented in Table 2 and Fig. 6. B/Ca data are species-specific and consistent with previous
469 work (e.g., compiled in Henehan et al., 2016) with ratios higher for *G. ruber* > *T. sacculifer* (sacc) > *T. sacculifer*
470 (w/o sacc) > *P. obliquiloculata* > *O. universa* > > *G. menardii* > *N. dutertrei* > *G. tumida* > *G. inflata* > *N.*
471 *pachyderma* > *G. bulloides* (Fig. 6). This study supports species-specific B/Ca ratios as previously published (Yu
472 et al., 2007; Tripathi et al., 2009, 2011; Allen and Hönisch, 2012; Henehan et al., 2016). Differences between
473 surface- and deep-dwelling foraminifera are observed, with lower values and a smaller range for the deeper-
474 dwelling taxa (58-126 $\mu\text{mol/mol}$ vs 83-190 $\mu\text{mol/mol}$ for shallow dwellers), however, the trend for the surface-
475 dwellers can also be driven by interspecies B/Ca variability. The B/Ca data for deep-dwelling taxa exhibits a
476 significant correlation with $[\text{B}(\text{OH})_4^-]/[\text{HCO}_3^-]$ ($p < 0.05$), but no correlation with $\delta^{11}\text{B}_{\text{carbonate}}$ and temperature (Fig.
477 S3). Surface-dwelling species have B/Ca ratios that exhibit significant correlations with $[\text{B}(\text{OH})_4^-]/[\text{HCO}_3^-]$,
478 $\delta^{11}\text{B}_{\text{carbonate}}$ and temperature. The sensitivity of B/Ca to $[\text{B}(\text{OH})_4^-]/[\text{HCO}_3^-]$ is lower for deep-dwelling species
479 compared to surface dwelling species. When all the B/Ca data are compiled, significant trends are observed with
480 $[\text{B}(\text{OH})_4^-]/[\text{HCO}_3^-]$, $\delta^{11}\text{B}_{\text{carbonate}}$ and temperature (Fig. S3). When comparing data from all sites together, a weak
481 decrease in B/Ca with increasing calcification depth is observed ($R^2=0.11$, $p < 0.05$, Fig. S4). A correlation also
482 exists between B/Ca and the water depths of the cores (not significant, Fig. S4).

483

484 5. Discussion

485

486 5.1 Sources of uncertainty relating to depth habitat and seasonality at studied sites

487

488 5.1.1 Depth habitats and $\delta^{11}\text{B}_{\text{borate}}$

489 Because foraminifera will record ambient environmental conditions during calcification, the accurate
490 characterization of *in situ* data is needed not only for calibrations, but also to understand the reconstructed record
491 of pH or $p\text{CO}_2$. The species we examined are ordered here from shallower to deeper depth habitats: *G. ruber* > *T.*
492 *sacculifer* (sacc) > *T. sacculifer* (w/o sacc) > *O. universa* > *P. obliquiloculata* > *G. menardii* > *N. dutertrei* > *G.*
493 *tumida* (this study; Birch et al., 2013; Farmer et al., 2007), although the specific water depth will vary depending
494 on the physical properties of the water column of the site (Kemle-von Mücke and Oberhänsli, 1999). We note that
495 calculation of absolute calcification depths can be challenging in some cases as many species often transition to
496 deeper waters at the end of their life cycle prior to gametogenesis (Steinhardt et al., 2015).

497 We find that assumptions about the specific depth habitat a species of foraminifera is calcifying over, in
498 a given region, can lead to differences of a few per mil in calculated isotopic compositions of borate (Fig. 3).

499 Hence this can cause a bias in calibrations if calcification depths are assumed instead of being calculated (i.e., with
500 $\delta^{18}\text{O}$ and/or Mg/Ca). Factors including variations in thermocline depth can impact depth habitats for some taxa.
501 At the sites we examined, most of the sampled species live in deeper depth habitats in the WEP relative to the
502 Indian Ocean, which in turn is characterized by deeper depth habitats than in the Arabian Sea. In the tropical
503 Pacific, *T. sacculifer* is usually found deeper than *G. ruber* except at sites characterized by a shallow thermocline,
504 in which case both species tend to overlap their habitat (e.g., ODP Site 806 in the WEP which has a deeper
505 thermocline than at ODP Site 847 in the Eastern Equatorial Pacific; EEP) (Rickaby et al., 2005). The difference in
506 depth habitats for *T. sacculifer* and *N. dutertrei* between the WEP and EEP can be as much as almost 100 m
507 (Rickaby et al., 2005).

508

509 **5.1.2 Seasonality and *in situ* $\delta^{11}\text{B}_{\text{borate}}$**

510 As discussed by Raitzsch et al. (2018), depending of the study area, foraminiferal fluxes can change
511 throughout the year. Hydrographic parameters related to carbonate chemistry may change across seasons at a given
512 water depth. We therefore recalculated the theoretical $\delta^{11}\text{B}_{\text{borate}}$ using seasonal data for temperature and salinity
513 and annual values for TA and DIC for each depth at each site. The GLODAP (2013) database does not provide
514 seasonal TA or DIC values.

515 The low sensitivity of $\delta^{11}\text{B}_{\text{borate}}$ to temperature and salinity means that calculated $\delta^{11}\text{B}_{\text{borate}}$ for each water
516 depth at our sites were not strongly impacted (Fig. S1). Thus, these findings support Raitzsch et al. (2018), who
517 concluded that calculated $\delta^{11}\text{B}_{\text{borate}}$ values corrected for seasonality was within error of non-corrected values for
518 each water depth. As Raitzsch et al. (2018) highlight, seasonality might be more important at high latitude sites
519 where seasonality is more marked, however, the seasonality of primary production will also be more tightly
520 constrained due to the seasonal progression of winter light limitation and intense vertical mixing and summer
521 nutrient limitation.

522 Data for our sites suggests that most $\delta^{11}\text{B}_{\text{borate}}$ variability we observe does not come from seasonality but
523 from the assumed water depths for calcification. With the exception of a few specific areas such as the Red Sea
524 (Henehan et al., 2016, Raitzsch et al., 2018), at most sites examined, seasonal $\delta^{11}\text{B}_{\text{borate}}$ at a fixed depth does not
525 vary by more than $\sim 0.2\%$. We conclude that seasonality has a relatively minor impact on the carbonate system
526 parameters at the sites we examined.

527

528 **5.2 $\delta^{11}\text{B}$, microenvironment pH and depth habitats**

529 It is common for planktonic foraminifera to have symbiotic relationships with algae (Gast and Caron,
530 2001; Shaked and de Vargas, 2006). The family Globigerinidae, including *G. ruber*, *T. sacculifer* and *O. universa*,
531 commonly have dinoflagellate algal symbionts (Anderson and Be, 1976; Spero, 1987). The families
532 Pulleniatinidae and Globorotaliidae (e.g. *P. obliquiloculata*, *G. menardii* and *G. tumida*) have chrysophyte algal
533 symbionts (Gastrich, 1988) and *N. dutertrei* hosts pelagophyte symbionts (Bird et al., 2018). The relationship
534 between the symbionts and the host is complex. Nevertheless, this symbiotic relationship provides energy
535 (Hallock, 1981b) and promotes calcification in foraminifera (Duguay, 1983; Erez et al., 1983) by providing
536 inorganic carbon to the host (Jorgensen et al., 1985).

537 There are several studies indicating that the $\delta^{11}\text{B}$ signatures in foraminiferal calcite reflect
538 microenvironment pH (Jorgensen et al., 1985; Rink et al., 1998; Köhler-Rink and Köhl, 2000, Hönisch et al., 2003;

539 Zeebe et al., 2003). Foraminifera with high photosynthetic activity and symbiont density, such as *G. ruber* and *T.*
540 *sacculifer*, are expected to have a microenvironment pH higher than ambient seawater, and a $\delta^{11}\text{B}_{\text{carbonate}}$ higher
541 than expected $\delta^{11}\text{B}_{\text{borate}}$, which is the case in our study and in previous studies (Foster et al., 2008, Henehan et al.,
542 2013, Raitzsch et al., 2018). We also observed in our study that *N. dutertrei*, *G. menardii*, *P. obliquiloculata* and
543 *G. tumida* record a lower pH than ambient seawater, with $\delta^{11}\text{B}_{\text{carbonate}}$ lower than expected $\delta^{11}\text{B}_{\text{borate}}$, and suggest
544 the results are consistent with lower photosynthetic activity compared to the mixed-layer dwelling species. These
545 observations, based on $\delta^{11}\text{B}_{\text{carbonate}}$ measurements, are in line with direct observations from Takagi et al. (2019)
546 that show dinoflagellate-bearing foraminifera (*G. ruber*, *T. sacculifer* and *O. universa*) tend to have a higher
547 symbiont density and photosynthesis activity while *P. obliquiloculata*, *G. menardii* and *N. dutertrei* have lower
548 symbiont density and *P. obliquiloculata*, *N. dutertrei* have the lowest photosynthetic activity. In the same study,
549 *P. obliquiloculata* exhibited minimum symbiont densities and levels of photosynthetic activity, which may explain
550 why *P. obliquiloculata* exhibited the lowest microenvironment pH as recorded by $\delta^{11}\text{B}$.

551 Based on the observations of Takagi et al. (2019), we can assume that the low $\delta^{11}\text{B}$ of *O. universa* and *T.*
552 *sacculifer* (w/o sacc) from the WEP is explained by low photosynthetic activity. It has been shown for *T. sacculifer*
553 and *O. universa* that symbiont photosynthesis increases with higher insolation (Jorgensen et al., 1985; Rink et al.,
554 1998) and the photosynthetic activity is therefore a function of the light level the symbionts received. This is, in a
555 natural system, dependent on the depth of the species in the water column. For the purpose of this study, we do
556 not consider turbidity which also influences the light penetration in the water column. In this case,
557 photosynthetically-active foraminifera living close to the surface should record microenvironment pH (thus $\delta^{11}\text{B}$)
558 that is more sensitive to water depth changes. A deeper habitat reduces solar insolation, and as a consequence, may
559 lower symbiont photosynthetic activity, possibly reducing pH in the foraminifera's microenvironment. This is
560 supported by the significant trend observed between $\Delta^{11}\text{B}$ and the calcification depth for *G. ruber* and *T. sacculifer*
561 at our sites (Fig. S2), where microenvironment pH decreases with calcification depth. We observe a significant
562 decrease in $\delta^{11}\text{B}$ in the WEP for *T. sacculifer* (w/o sacc) compared to the other sites ($p < 0.05$). Additionally, the
563 $\Delta^{11}\text{B}$ ($\Delta^{11}\text{B} = \delta^{11}\text{B}_{\text{carbonate}} - \delta^{11}\text{B}_{\text{borate}}$) of *G. ruber*, *T. sacculifer* (w/o sacc and sacc) is significantly lower in the
564 WEP compared to the other sites ($p < 0.05$).

565 *T. sacculifer* has the potential to support more photosynthesis due to its higher symbiont density, and
566 higher photosynthetic activity compared to other species, which may support higher symbiont/host interactions
567 (Takagi et al., 2019). These results would be consistent with a greater sensitivity of *T. sacculifer*'s photosynthetic
568 activity with changes in insolation/water depth. To test if the low $\delta^{11}\text{B}$ signature of *T. sacculifer* (w/o sacc) in the
569 WEP is related to a decrease in light at greater water depth, we have independently calculated the calcification
570 depth of the foraminifera based on various light insolation culture experiments (Jorgensen et al., 1985) and the
571 microenvironment ΔpH derived from our data (Fig. 7A and B). This exercise showed that the low $\delta^{11}\text{B}$ of *T.*
572 *sacculifer* (w/o sacc) from the WEP can be explained by the reduced light environment due to a deeper depth
573 habitat in the WEP (Fig. 7B). It can also be noted that *T. sacculifer* exhibits the largest variation in symbiont
574 density versus test size (Takagi et al., 2019), suggesting that lower size fraction reported for the WEP (250-400
575 μm) compared to the 300-400 μm at the other sites can be related to a decrease in photosynthetic activity and a
576 lower $\delta^{11}\text{B}$. Unfortunately, no weight per shell data were determined on foraminifera samples to constrain whether
577 test size was significantly different across sites. Future studies could use shell weights to test these relationships.

578 When the same approach of independently reconstructing calcification depth based on culture
579 experiments is applied to *O. universa*, the boron data suggest a microenvironment pH of 0.10 to 0.20 lower than
580 ambient seawater pH, which would be in line with the species living deeper than 50m (light compensation point
581 (Ec), Rink et al., 1998), which is consistent with our calcification depth reconstructions. The low $\delta^{11}\text{B}_{\text{carbonate}}$ of
582 *O. universa* compared to *T. sacculifer* for the similar calcification depth at some sites (e.g. FC-02a, WP07-a) might
583 reflect differences in photosynthetic potential between the two species, which is supported by observation of a
584 lower photosynthetic potential in *O. universa* than in *T. sacculifer* (Tagaki et al., 2019).

585 Microenvironment ΔpH based on our $\delta^{11}\text{B}_{\text{carbonate}}$ data were calculated for the rest of the species. We
586 observed that microenvironment ΔpH is higher in *T. sacculifer* > *G. ruber* > *T. sacculifer* (w/o sacc - WEP) > *O.*
587 *universa*, *N. dutertrei*, *G. menardii*, *G. tumida* > *P. obliquiloculata*. These results are in line with the
588 photosymbiosis findings from Takagi et al., (2019). Also, the higher $\delta^{11}\text{B}$ data from the West African upwelling
589 published by Raitzsch et al., (2018) for *G. ruber* and *O. universa* may reflect a higher microenvironment pH due
590 to a relatively shallow habitat, higher insolation and high rates of photosynthesis by symbionts. This could
591 highlight a potential issue with calibration when applied to sites with different oceanic regimes as the $\delta^{11}\text{B}$ species-
592 specific calibrations could be also location-specific for the mixed dweller species.

593 Microenvironment pH for *N. dutertrei*, *G. menardii* and *G. tumida* are similar to *O. universa* and suggest
594 a threshold for a respiration-driven $\delta^{11}\text{B}$ signature. This threshold can be induced by a change of photosynthetic
595 activity at lower light intensity in deeper water and/or differences in symbiont density and/or by the type of
596 symbionts at greater depth (non-dinoflagellate symbionts). We also note that *P. obliquiloculata*, which has the
597 lowest symbiont density and photosynthetic activity (Takagi et al., 2019), has the lowest microenvironment pH
598 compared to other deeper-dweller species, supporting our hypothesis that respiration can control
599 microenvironment pH. The deep-dwelling species sensitivity of $\delta^{11}\text{B}_{\text{carbonate}}$ to $\delta^{11}\text{B}_{\text{borate}}$ with values close to unity
600 might also be explained by a relatively stable respiration-driven microenvironments, as the deeper-dweller species
601 do not experience large changes of insolation (e.g. photosynthesis), thereby making them a more direct recorder
602 of environmental pH.

603

604 **5.3 $\delta^{11}\text{B}$ sensitivity to $\delta^{11}\text{B}_{\text{borate}}$ and relationship with B/Ca signatures**

605 In inorganic calcite, $\delta^{11}\text{B}_{\text{carbonate}}$ and B/Ca data have shown to be sensitive to precipitation rate with at
606 higher precipitation rate increasing $\delta^{11}\text{B}_{\text{carbonate}}$ (Farmer et al., 2019) and B/Ca (Farmer et al., 2019; Gabitov et al.,
607 2014; Kaczmarek et al., 2016; Mavromatis et al., 2015; Uchikawa et al., 2015). A recent study from Farmer et al,
608 (2019) has proposed that in foraminifera at higher precipitation rates, more borate ion may be incorporated into
609 the carbonate mineral, while more boric acid may be incorporated at lower precipitation rates. The authors also
610 suggest this may explain low sensitivities of culture experiments.

611 When combining all literature data, *T. sacculifer* and *G. ruber* have sensitivities of $\delta^{11}\text{B}_{\text{carbonate}}$ to $\delta^{11}\text{B}_{\text{borate}}$
612 of 0.83 ± 0.48 and 0.46 ± 0.34 respectively in line with previous literature and paleo- CO_2 reconstructions. Also, if
613 we only take into account our data, and the observation that the sensitivity of $\delta^{11}\text{B}_{\text{carbonate}}$ to $\delta^{11}\text{B}_{\text{borate}}$ is not
614 statistically different from unity for most of the species investigated, we can speculate that for these taxa, changes
615 in precipitation rate and contributions of boric acid are not likely to be important. If considering only the data from
616 this study, *G. ruber* (1.12 ± 1.67) and *T. sacculifer* (1.38 ± 1.35) present higher sensitivities of $\delta^{11}\text{B}_{\text{carbonate}}$ to
617 $\delta^{11}\text{B}_{\text{borate}}$. We can then again speculate that the observed high values for $\delta^{11}\text{B}_{\text{carbonate}}$ at high seawater pH can be due

618 to higher precipitation rates. We note this could also be consistent with the higher sensitivity of B/Ca signatures
619 in these two surface dwelling species to ambient $[B(OH)_4^-]/[HCO_3^-]$ relative to deeper-dwelling species. Those
620 interspecific differences still remain to be explained, however, part of this variability is likely due to changes in
621 the carbonate chemistry of the microenvironment resulting in changing competition between borate and
622 bicarbonate. A caveat is that we can not exclude specific biological processes, and that in taxa with a non
623 respiration-driven microenvironment, changes in day/night calcification ratios also impacting observed values. As
624 indicated by Farmer et al., (2019), studies of calcite precipitation rates in foraminifera may help to improve our
625 understanding of the fundamental basis of boron-based proxies.

626

627 **5.4 Evaluation of species for pH reconstructions and water depth pH reconstructions**

628 This data set allows us to reassess the utility of boron-based proxies for the carbonate system. The main
629 aim of using boron-based proxies relates to the reconstruction of past oceanic conditions, specifically pH and
630 pCO₂. Mixed-layer species (eg. *G. ruber* and *T. sacculifer*) are potential archives for atmospheric CO₂
631 reconstructions. Other species can shed light on other aspects of the carbon cycle including the physical and
632 biological carbon pumps.

633 There are a few main inferences we can make. When integrated with published data, the sensitivities of
634 $\delta^{11}B_{\text{carbonate}}$ to $\delta^{11}B_{\text{borate}}$ for *G. ruber* and *T. sacculifer* are similar to previous studies (Martinez-Boti et al., 2015b;
635 Raitzsch et al., 2018) which supports the fidelity of previous paleo-reconstructions that use published calibrations
636 between $\delta^{11}B_{\text{carbonate}}$ and $\delta^{11}B_{\text{borate}}$. The regression we have made for *G. ruber* supports a decrease in $\delta^{11}B_{\text{carbonate}}$
637 with decreasing size fractions (offset of -0.4 ‰, p>0.05) with the sensitivity of $\delta^{11}B_{\text{carbonate}}$ to $\delta^{11}B_{\text{borate}}$ not being
638 statistically different from higher size fraction (p<0.05). The variability in our weight per shell for our *G. ruber*,
639 based data from Henehan et al. (2013), can potentially imply a deviation down to 1‰ relative to calibration line
640 from Henehan et al. (2013), which can be in line with the maximum deviation observed in our data (~1.2 ‰) and
641 not inconsistent with a size effect explaining the offset in our calibration. Our $\delta^{11}B_{\text{carbonate}}$ data and the sensitivity
642 to $\delta^{11}B_{\text{borate}}$ of *O. universa* supports previous data from Henehan et al. (2016). *N. dutertrei* $\delta^{11}B_{\text{carbonate}}$ data span a
643 large range of pH, allowing us to derive a robust calibration with $\delta^{11}B_{\text{borate}}$. It remains premature to assume that a
644 unique calibration with a slope of ~-0.9 can be used for all deeper-dwelling species, more data is needed for *P.*
645 *obliquiloculata*, *G. menardii* and *G. tumida* to robustly test this assertion.

646 In order to derive accurate reconstructions of past ambient pH and pCO₂, accurate species-specific
647 calibrations need to be used that are constrained by core-tops or samples from similar types of settings (Fig. 8, 10,
648 S6). Lower $\delta^{11}B$ signatures in *T. sacculifer* (w/o sacc) are observed in the WEP, which may be explained by the
649 deeper depth habitat for this taxa, as lower light levels might reduce symbiont photosynthetic activity. Also, we
650 show that a correction is needed for *T. sacculifer* (w/o sacc) in the WEP in order to accurately reconstruct
651 atmospheric CO₂. When applying calibrations n°2 and 4 to *T. sacculifer* and *G. ruber* (compilation of all data,
652 Table 3) our data show more variability, especially for *G. ruber* which lead to the larger mismatch compared to *in*
653 *situ* parameters. The greater divergence of reconstructed values from *in situ* measurements are observed at site
654 WPO7-01 for both *T. sacculifer* (w/o sacc) and *G. ruber*. More data would be needed to determine a proper
655 correction for both species and coretop study will be determinant for future downcore reconstructions, especially
656 in the WEP. We also find that for two species, the boron isotope-pH proxy is a relatively straightforward recorder
657 of ambient pH, with sensitivities close to unity observed for *O. universa* and *N. dutertrei*.

658 There is also promise in using multiple species in a sample from different hydrographic regimes to
659 reconstruct vertical profiles of pH and pCO₂. We are able to reproduce pH and pCO₂ profiles from multiple sites
660 with different water column structures (Fig. 8) with those reconstructions within error of the *in situ* values, for
661 most sites. In order to avoid circularity, to validate these calibrations, we recalculated ambient pH and pCO₂ by
662 first excluding site-specific data and then recalculating species-specific calibrations, followed by application to
663 each specific site. The comparison of the two methods, first using all the data to derive the calibration and
664 recalculate pH and pCO₂ (circular) and the second by excluding the site of interest, derive calibrations and calculate
665 pH and pCO₂ (not circular), does not show significant differences and validates the robustness of the calibrations
666 (Fig. S5). We utilized the calibrations derived from our data for *G. ruber* (calibration n°1 and 2, Table 3), *T.*
667 *sacculifer* (calibration n°3 and 4, Table 3), *O. universa* (calibration n°8, Table 3), for *P. obliquiloculata* (calibration
668 n°11, Table 3), and for *N. dutertrei*, *G. tumida* and *G. menardii* the calibration made on the compilation of the
669 deep-dweller (calibration n°13, Table 3). Results are shown in Fig. 8 and evaluated in Fig. 9. For *G. menardii*,
670 more data would be helpful to provide additional constraints. Results for *G. ruber* are the most scattered,
671 potentially due to difference in test sizes (Henehan et al., 2013), or depth habitat. Results reaffirm the importance
672 of working with narrow size fractions (Henehan et al., 2013), the utilization of calibrations derived from the same
673 size fraction or use of offsets to take into account this size fraction effect, and the importance of core-top studies
674 before paleo-application.

675

676 **6. Conclusions and future implications**

677 Our study has extended the boron isotope proxy with data for new species and sites. The work supports
678 previous work showing that depth habitats of foraminifera vary depending on the oceanic regime, and this can
679 impact boron isotope signatures. Low δ¹¹B values in the WEP compared to other regions for *T. sacculifer* (w/o
680 sacc) may be explained by a reduction in microenvironment pH due to a deeper depth habitat associated with
681 reduced irradiance and thus photosynthetic activity.

682 In order to accurately develop downcore reconstructions, constraining the depth habitat using core-tops
683 studies is important, as a same species can record the seawater pH at different water depth potentially introducing
684 biases when comparing between different locations. Also, we speculate that a change of the thermocline depth in
685 the past could imply variations of depth habitat and introduce biases in the reconstructions but further work is
686 needed to test this assertion.

687 The sensitivity of δ¹¹B_{carbonate} to pH is in line with previously published data for *T. sacculifer*, *G. ruber*.
688 The sensitivity of δ¹¹B_{carbonate} to pH of *O. universa* (mixed-dweller), *N. dutertrei*, *G. menardii* and *G. tumida* (deep-
689 dwellers) are similar but more data are needed to fully determine those sensitivities. The similarity of boron isotope
690 calibrations for deep-dwelling taxa might be related to similar respiration-driven microenvironments.

691 Reconstruction of seawater pH and carbonate system parameters is achievable using foraminiferal δ¹¹B
692 but additional core-top and down-core studies reconstructing depth profiles will be needed in order to further verify
693 calibrations published to date. Past pH and pCO₂ water depth profiles can potentially be created by utilizing
694 multiple foraminiferal species in concert with taxon-specific calibrations for similar settings. This approach has
695 much potential for enhancing our understanding of the past workings of the oceanic carbon cycle, and the
696 biological pump.

697

698 **Author contribution**

699 R.E and A.T. wrote the proposals that funded the work. A.T. and F.C. provided the samples. M.G., S.M. and A.T.
700 contributed to the experimental design. A.V. helped for sample preparation. M.G. and S.M contributed to
701 developing the method of boron isotope analysis. M.G. performed the measurements with assistance from S.M.
702 M.G conducted the data analysis. M.G. drafted the paper, which was edited by all authors. Interpretation was led
703 by M.G., A.T., S.M. with input from R.E., A.V. and F.C.

704

705 **Competing interests**

706 The authors declare that they have no conflict of interest.

707

708 **Acknowledgments:**

709 The authors wish to thank Jesse Farmer for his valuable and detailed comments on the actual and a previous version
710 of the manuscript. We wish to thank Michael Henehan for helpful discussion, comments on the manuscript and
711 help with the code. We also want to thank the anonymous reviewer for helpful comments. Lea Bonnin for
712 assistance with picking samples, the IODP repository for provision of samples, the Tripati Laboratory (UCLA) for
713 their technical support, Mervyn Greaves, Madeleine Bohlin (University of Cambridge) for technical support and
714 use of laboratory space, Yoan Germain, Emmanuel Ponzevera and Oanez Lebeau for technical support and use of
715 laboratory space in Brest, Jill Sutton for helpful conversation on the manuscript. Research is supported by DOE
716 BES grant DE-FG02-13ER16402, by the International Research Chair Program that is funded by the French
717 government (LabexMer ANR-10-LABX-19-01), and IAGC student research grant 2017.

718

719 **References**

- 720 Allen, K. A. and Hönisch, B.: The planktic foraminiferal B/Ca proxy for seawater carbonate chemistry, A critical
721 evaluation, *Earth Planet. Sci. Lett.*, 345–348, 203–211, 2012.
- 722 Anagnostou, E., John, E., Edgar, K., Foster, G., Ridgwell, A., Inglis, G., Pancost, R., Lunt, D. and Pearson, P.,
723 Changing atmospheric CO₂ concentration was the primary driver of early Cenozoic climate: *Nature* 533,
724 380–384, 2016.
- 725 Anand, P., Elderfield, H. and Conte, M. H., Calibration of Mg/Ca thermometry in planktonic foraminifera from a
726 sediment trap time series. *Paleoceanography* 18, 2003.
- 727 Anderson, O. R. and Bé, A.W. H.: The ultrastructure of a planktonic foraminifer, *Globigerinoides sacculifer*
728 (Brady), and its symbiotic dinoflagellates: *J. Foramin. Res.*, 6, 1–21, 1976.
- 729 Axelsson, M. D., Rodushkin, I., Ingri, J. and Öhlander, B.: Multielemental analysis of Mn–Fe nodules by ICP-
730 MS: optimisation of analytical method, *Analyst*, 127, 76–82, 2002.
- 731 Babila, T.L., Rosenthal, Y., Conte, M.H.: Evaluation of the biogeochemical controls on B/Ca of *Globigerinoides*
732 *ruber* white from the Oceanic Flux Pro-gram, Bermuda, *Earth Planet. Sci. Lett.* 404, 67–76, 2014.
- 733 Barker, S., Greaves M. and Elderfield, H.: A study of cleaning procedures used for foraminiferal Mg/Ca
734 paleothermometry, *Geochemistry, Geophys. Geosystems* 4, 1–20, 2003.
- 735 Bartoli, G., Hönisch, B. and Zeebe, R. E.: Atmospheric CO₂ decline during the Pliocene intensification of
736 Northern Hemisphere glaciations, *Paleoceanography* 26, 1–14, 2011.
- 737 Bemis, B. E., Spero, H. J., Bijma, J. and Lea, D. W.: Reevaluation of the oxygen isotopic composition of
738 planktonic foraminifera: Experimental results and revised paleotemperature equations, *Paleoceanography*
739 13, 150–160, 1998.
- 740 Bemis, B. E., Spero, H. J. and Thunell, R. C.: Using species-specific paleotemperature equations with
741 foraminifera: a case study in the Southern California Bight, *Mar. Micropaleontol.*, 46, 405–430, 2002.
- 742 Bijma, J., Faber Jr., W.W., Hemleben, C.: Temperature and salinity limits for growth and survival of some
743 planktonic foraminifera in laboratory cultures, *J. Foraminiferal Res.* 20 (2), 95–116, 1990.
- 744 Bijma, J., Hönisch, B. and Zeebe, R. E.: Impact of the ocean carbonate chemistry on living foraminiferal shell
745 weight: Comment on “Carbonate ion concentration in glacial-age deep waters of the Caribbean Sea” by W.
746 S. Broecker and E. Clark, *Geochemistry, Geophys. Geosystems*, 3, 1–7, 2002.
- 747 Birch, H., Coxall, H. K., Pearson, P. N., Kroon, D. and O’Regan, M.: Planktonic foraminifera stable isotopes and
748 water column structure, Disentangling ecological signals, *Mar. Micropaleontol.*, 101, 127–145, 2013.
- 749 Bird, C., Darling, K. F., Russell, A. D., Fehrenbacher, J. S., Davis, C. V., Free, A., & Ngwenya, B. T.: 16S
750 rRNA gene metabarcoding and TEM reveals different ecological strategies within the genus
751 *Neogloboquadrina* (planktonic foraminifer), *PloS one*, 13(1), 2018.
- 752 Boyer, T.P., Antonov, J. I., Baranova, O. K., Coleman, C., Garcia, H. E., Grodsky, A., Johnson, D. R., Locarnini,
753 R. A., Mishonov, A. V., O’Brien, T.D., Paver, C.R., Reagan, J.R., Seidov, D., Smolyar, I. V., and Zweng,
754 M. M.: *World Ocean Database*, NOAA Atlas NESDIS 72, S. Levitus, Ed., A. Mishonov, Technical Ed.,
755 Silver Spring, MD, 209, 2013.
- 756 Boyle, E. A., Cadmium, zinc, copper, and barium in foraminifera tests, *Earth Planet. Sci. Lett.*, 53, 11–35, 1981.

- 757 Boyle, E. A., and L. D., Keigwin, Comparison of Atlantic and Pacific paleochemical records for the Last
758 215,000 years: Changes in deep ocean circulation and chemical inventories, *Earth Planet. Sci. Lett.*, 76,
759 135–150, 1985.
- 760 Branson, O., Kaczmarek, K., Redfern, S. A. T., Misra, S., Langer, G., Tyliszczak, T., Bijma, J. and Elderfield,
761 H., The coordination and distribution of B in foraminiferal calcite, *Earth Planet. Sci. Lett.*, 416, 67–72,
762 2015.
- 763 Catanzaro, E.J., Champion, C.E., Garner, A.L., Marinenko, G., Sappenfield, K.M. and Shields, W.R.: Boric
764 Acid; Isotopic and Assay Standard Reference Materials, U.S. Natl. Bur. Stand. Spec., Publ. 260-17, 70p,
765 1970.
- 766 Chalk, T. B., Hain, M. P., Foster, G. L., Rohling, E. J., Sexton, P. F., Badger, M. P. S., Cherry, S. G., Hasenfratz,
767 A. P., Haug, G. H., Jaccard, S. L., Martínez-García, A., Pälike, H., Pancost, R. D. and Wilson, P. A.,
768 Causes of ice age intensification across the Mid-Pleistocene Transition, *Proc. Natl. Acad. Sci.*, 114,
769 13114–13119, 2017.
- 770 Coadic, R., Bassinot, F., Dissard, D., Douville, E., Greaves, M. and Michel, E., A core-top study of dissolution
771 effect on B/Ca in Globigerinoides sacculifer from the tropical Atlantic: Potential bias for paleo-
772 reconstruction of seawater carbonate chemistry, *Geochemistry, Geophys. Geosystems* 14, 1053–1068,
773 2013.
- 774 de Nooijer, L. J., Spero, H. J., Erez, J., Bijma, J. and Reichart, G. J., Biomineralization in perforate foraminifera.
775 *Earth-Science Rev.*, 135, 48–58, 2014.
- 776 Dekens, P. S., Lea, D. W., Pak, D. K. and Spero, H. J., Core top calibration of Mg/Ca in tropical foraminifera,
777 Refining paleotemperature estimation, *Geochemistry, Geophys. Geosystems* 3, 1–29, 2002.
- 778 Deuser, W.G., Ross, E.H., Hemleben, Ch., Spindler, M., Seasonal changes in species composition, numbers,
779 mass, size, and isotopic composition of planktonic foraminifera settling into the deep Sargasso Sea,
780 *Palaeogeogr., Palaeoclimat., Palaeoecol.*, 33:103-127, 1981.
- 781 Deuser, W. G. and Ross, E. H., Seasonally abundant planktonic foraminifera of the Sargasso Sea; succession,
782 deep-water fluxes, isotopic compositions, and paleoceanographic implications, *J. Foraminifer. Res.* 19,
783 268–293, 1989.
- 784 Dickson, A. G., Thermodynamics of the dissociation of boric acid in synthetic seawater from 273.15 to 318.15
785 K., *Deep Sea Res., Part A, Oceanogr. Res. Pap.* 37, 755–766, 1990.
- 786 Dickson, A.G., Millero, F.J., A comparison of the equilibrium constants for the dissociation of carbonic acid in
787 seawater media, *Deep-Sea Res.*, 34, 1733–1743, 1987.
- 788 Douville, E., Paterne, M., Cabioch, G., Louvat, P., Gaillardet, J., Juillet-Leclerc, A. and Ayliffe, L., Abrupt sea
789 surface pH change at the end of the Younger Dryas in the central sub-equatorial Pacific inferred from
790 boron isotope abundance in corals (*Porites*), *Biogeosciences* 7, 2445–2459, 2010.
- 791 Duguay, L.E., Comparative laboratory and field studies on calcification and carbon fixation in foraminiferal-
792 algal associations, *Journal of Foraminiferal Research* 13, 252-261, 1983.
- 793 Duplessy, J., Labeyrie, L., Juilletleclerc, A., Maitre, F., Duprat, J. and Sarnthein, M.: Surface salinity
794 reconstruction of the north-atlantic ocean during the last glacial maximum, *Oceanol. Acta*, 14, 311–324,
795 1991.
- 796 Elderfield, H., Yu, J., Anand, P., Kiefer, T. and Nyland, B., Calibrations for benthic foraminiferal Mg/Ca
797 paleothermometry and the carbonate ion hypothesis, *Earth Planet. Sci. Lett.*, 250, 633–649., 2006.

- 798 Elderfield, H. and Granssen, G., Past temperatures and O18 of surface ocean waters inferred from foraminiferal
799 Mg/Ca ratios, *Nature* 405, 442–445, 2000.
- 800 Erez J., Calcification Rates, Photosynthesis and Light in Planktonic Foraminifera. In: Westbroek P., de Jong
801 E.W. (eds) *Biom mineralization and Biological Metal Accumulation*. Springer, Dordrecht, 1983.
- 802 Erez, J., The Source of Ions for Biom mineralization in Foraminifera and Their Implications for Paleoceanographic
803 Proxies, *Rev. Mineral. Geochemistry*, 54, 115–149, 2003.
- 804 Fairbanks, R. G. and Wiebe, P. H.: Foraminifera and Chlorophyll Maximum: Vertical Distribution, Seasonal
805 Succession, and Paleoceanographic Significance, *Science*, 209, 1524–1526, 1980.
- 806 Fairbanks, R. G., Sverdløve, M., Free, R., Wiebe, P. H. and Bé, A. W. H.: Vertical distribution and isotopic
807 fractionation of living planktonic foraminifera from the Panama Basin, *Nature*, 298, 841–844, 1982.
- 808 Farmer, E. C., Kaplan, A., de Menocal, P. B. and Lynch-Stieglitz, J., Corroborating ecological depth preferences
809 of planktonic foraminifera in the tropical Atlantic with the stable oxygen isotope ratios of core top
810 specimens, *Paleoceanography*, 22, 1–14, 2007.
- 811 Farmer, J. R., Hönisch, B., & Uchikawa, J.: Single laboratory comparison of MC-ICP-MS and N-TIMS boron
812 isotope analyses in marine carbonates, *Chemical Geology*, 447, 173–182, 2016.
- 813 Farmer, J. R., Branson, O., Uchikawa, J., Penman, D. E., Hönisch, B., & Zeebe, R. E.: Boric acid and borate
814 incorporation in inorganic calcite inferred from B/Ca, boron isotopes and surface kinetic modeling,
815 *Geochimica et Cosmochimica Acta*, 244, 229–247, 2019.
- 816 Feely, R., Impact of Anthropogenic CO₂ on the CaCO₃ System in the Oceans, *Science*, 305, 362–366, 2004.
- 817 Ferguson, J. E., Henderson, G. M., Kucera, M. and Rickaby, R. E. M.: Systematic change of foraminiferal
818 Mg/Ca ratios across a strong salinity gradient, *Earth Planet. Sci. Lett.*, 265, 153–166, 2008.
- 819 Foster, G. L., Seawater pH, pCO₂ and [CO₃²⁻] variations in the Caribbean Sea over the last 130 kyr: A boron
820 isotope and B/Ca study of planktic foraminifera, *Earth Planet. Sci. Lett.*, 271, 254–266, 2008.
- 821 Foster, G. L. and Sexton, P. F.: Enhanced carbon dioxide outgassing from the eastern equatorial Atlantic during
822 the last glacial, *Geology*, 42, 1003–1006, 2014.
- 823 Foster, G. L., Lear, C. H. and Rae, J. W. B., The evolution of pCO₂, ice volume and climate during the middle
824 Miocene, *Earth Planet. Sci. Lett.*, 341–344, 243–254, 2012.
- 825 Foster, G. L. and Rae, J. W. B., Reconstructing Ocean pH with Boron Isotopes in Foraminifera, *Annu. Rev.*
826 *Earth Planet. Sci.*, 44, 207–237, 2016.
- 827 Gabitov, R. I., Rollion-bard, C., Tripathi, A. and Sadekov, A., In situ study of boron partitioning between calcite
828 and fluid at different crystal growth rates, *Geochim. Cosmochim. Acta*, 137, 81–92, 2014.
- 829 Gaillardet, J., Lemarchand, D., Göpel, C. and Manhès, G., Evaporation and Sublimation of Boric Acid :
830 Application for Boron Purification from Organic Rich Solutions, *Geostand. Newsl.*, 25, 67–75, 2001.
- 831 Gast, R. J. and Caron D. A., Photosymbiotic associations in planktonic foraminifera and radiolaria, 1–7, 2001.
- 832 Gastrich, M.D., Ultrastructure of a new intracellular symbiotic alga found within planktonic foraminifera,
833 *Journal of Phycology* 23, 623–632, 1988.
- 834 Gattuso, J.P. and Hansson, L., *Ocean acidification*, Oxford University Press, 2011.

- 835 Gutjahr, M., Bordier, L., Douville, E., Farmer, J., Foster, G. L., Hathorne, E., Hönisch, B., Lemarchand, D., Louvat,
836 P., McCulloch, M., Noireaux, J., Pallavicini, N., Rodushkin, I., Roux, P., Stewart, J., Thil, F. You, C.F.,
837 Boron Isotope Intercomparison Project (BIIP): Development of a new carbonate standard for stable isotopic
838 analyses. In EGU general assembly conference abstracts, Vol. 16, (2014).
- 839 Hallock P., Algal Symbiosis : A Mathematical Analysis Marine Biology 62, 249-255, 1981b.
- 840 Hemming, N. G. and Hanson, G. N. Boron isotopic composition and concentration in modern marine carbonates,
841 Geochim. Cosmochim. Acta, 56, 537–543, 1992.
- 842 Hendry, K.R., Rickaby, R.E.M., Meredith, M.P., Elderfield, H., Controls on stable isotope and trace metal
843 uptake in *Neogloboquadrina pachyderma* (sinistral) from an Antarctic sea-ice environment. Earth Planet.
844 Sci. Lett. 278, 67–77, 2009.
- 845 Henehan, M. J., Foster, G. L., Bostock, H. C., Greenop, R., Marshall, B. J. and Wilson, P. A., A new boron
846 isotope-pH calibration for *Orbulina universa*, with implications for understanding and accounting for ‘vital
847 effects’, Earth Planet. Sci. Lett., 454, 282–292, 2016.
- 848 Henehan, M. J., Foster, G. L., Rae, J. W. B., Prentice, K. C., Erez, J., Bostock, H. C., Marshall, B. J. and Wilson,
849 P. A., Evaluating the utility of B/Ca ratios in planktic foraminifera as a proxy for the carbonate system: A
850 case study of *Globigerinoides ruber*, Geochemistry, Geophys. Geosystems 16, 1052–1069, 2015.
- 851 Henehan, M. J., Rae, J. W. B., Foster, G. L., Erez, J., Prentice, K. C., Kucera, M., Bostock, H. C., Martínez-Botí,
852 M. A., Milton, J. A., Wilson, P. A., Marshall, B. J. and Elliott, T., Calibration of the boron isotope proxy in
853 the planktonic foraminifera *Globigerinoides ruber* for use in palaeo-CO₂ reconstruction, Earth Planet. Sci.
854 Lett. 364, 111–122, 2013.
- 855 Holcomb, M., Decarlo, T. M., Schoepf, V., Dissard, D., Tanaka, K. and McCulloch, M.: Cleaning and pre-
856 treatment procedures for biogenic and synthetic calcium carbonate powders for determination of elemental
857 and boron isotopic compositions, Chem. Geol., 398, 11–21, 2015.
- 858 Hönisch, B., Hemming, N. G., Archer, D., Siddall, M. and McManus, J. F., Atmospheric Carbon Dioxide
859 Concentration Across the Mid-Pleistocene Transition, Science, 324, 1551–1554, 2009.
- 860 Hönisch, B., Bijma, J., Russell, A. D., Spero, H. J., Palmer, M. R., Zeebe, R. E. and Eisenhauer, A., The
861 influence of symbiotic photosynthesis on the boron isotopic composition of foraminifera shells, Mar.
862 Micropaleontol., 49, 87–96, 2003.
- 863 Hönisch, B. and Hemming, N. G., Ground-truthing the boron isotope-paleo-pH proxy in planktonic foraminifera
864 shells: Partial dissolution and shell size effects, Paleoceanography 19, 1–13, 2004.
- 865 Hönisch, B., Bickert, T. and Hemming, N. G., Modern and Pleistocene boron isotope composition of the benthic
866 foraminifer *Cibicides wuellerstorfi*, Earth Planet. Sci. Lett., 272, 309–318, 2008.
- 867 Howes, E. L., Kaczmarek, K., Raitzsch, M., Mewes, A., Bijma, N., Horn, I., Misra, S., Gattuso, J. P. and Bijma,
868 J., Decoupled carbonate chemistry controls on the incorporation of boron into *Orbulina universa*,
869 Biogeosciences, 14, 415–430, 2017.
- 870 IPCC: Climate Change 2014 - The Physical Science Basis, edited by Intergovernmental Panel on Climate
871 Change, Cambridge University Press, Cambridge., 2014.
- 872 Jørgensen, B. B., Erez, J., Revsbech, P. and Cohen, Y., Symbiotic photosynthesis in a planktonic foraminifera,
873 *Globigerinoides sacculifer* (Brady), studied with microelectrodes, Limnol. Oceanogr., 30, 1253–1267
874 1985.

- 875 Kaczmarek, K., Nehrke, G., Misra, S., Bijma, J. and Elderfield, H., Investigating the effects of growth rate and
876 temperature on the B/Ca ratio and $\delta^{11}\text{B}$ during inorganic calcite formation, *Chem. Geol.*, 421, 81–92,
877 2016.
- 878 Kemle-von Mücke S. and Oberhänsli H., The Distribution of Living Planktic Foraminifera in Relation to
879 Southeast Atlantic Oceanography, *Use Proxies Paleocenoogr.*, 91–115, 1999.
- 880 Key, R.M., A global ocean carbon climatology: Results from Global Data Analysis Project (GLODAP), *Global*
881 *Biogeochem. Cycles*, 18, GB4031, 2004.
- 882 Kim, S.T. and O’Neil, J. R., Equilibrium and nonequilibrium oxygen isotope effects in synthetic carbonates,
883 *Geochim. Cosmochim. Acta*, 61, 3461–3475, 1997.
- 884 Klochko, K., Cody, G. D., Tossell, J. A., Dera, P. and Kaufman, A. J., Re-evaluating boron speciation in
885 biogenic calcite and aragonite using ^{11}B MAS NMR, *Geochim. Cosmochim. Acta*, 73, 1890–1900, 2009.
- 886 Klochko, K., Kaufman, A. J., Yao, W., Byrne, R. H. and Tossell, J. A., Experimental measurement of boron
887 isotope fractionation in seawater, *Earth Planet. Sci. Lett.*, 248, 276–285, 2006.
- 888 Köhler-Rink, S. and Kühn, M., Microsensor studies of photosynthesis and respiration in larger symbiotic
889 foraminifera. I. The physico-chemical microenvironment of *Marginopora vertebralis*, *Amphistegina*
890 *lobifera* and *Amphisorus hemrichii*, *Mar. Biol.*, 137, 473–486, 2000.
- 891 Köhler-Rink, S. and Kühn, M., Microsensor studies of photosynthesis and respiration in the larger symbiont
892 bearing foraminifera *Amphistegina lobifera*, and *Amphisorus hemprichii*, *Ophelia*, 55, 111–122, 2001.
- 893 Lea, D. W., Pak, D. K. and Spero, H. J., Climate impact of late quaternary equatorial Pacific sea surface
894 temperature variations, *Science*, 289, 1719–1724, 2000.
- 895 Lemarchand, D., Gaillardet, J., Lewin, A. and Allègre, C. J., Boron isotope systematics in large rivers:
896 Implications for the marine boron budget and paleo-pH reconstruction over the Cenozoic, *Chem. Geol.*,
897 190, 123–14, 2002.
- 898 Liu, Y., Liu, W., Peng, Z., Xiao, Y., Wei, G., Sun, W., He, J., Liu, G. and Chou, C.L., Instability of seawater pH
899 in the South China Sea during the mid-late Holocene: Evidence from boron isotopic composition of corals,
900 *Geochim. Cosmochim. Acta*, 73, 1264–1272, 2009.
- 901 Lloyd, N. S., Sadekov, A. Y. and Misra, S., Application of 1013ohm Faraday cup current amplifiers for boron
902 isotopic analyses by solution mode and laser ablation multicollector inductively coupled plasma mass
903 spectrometry, *Rapid Commun. Mass Spectrom.*, 32, 9–18, 2018.
- 904 Martínez-Botí, M. A., Foster, G. L., Chalk, T. B., Rohling, E. J., Sexton, P. F., Lunt, D. J., Pancost, R. D.,
905 Badger, M. P. S. and Schmidt, D. N., Plio-Pleistocene climate sensitivity evaluated using high-resolution
906 CO₂ records, *Nature*, 518, 49–54, 2015a.
- 907 Martínez-Botí M. A., Marino G., Foster G. L., Ziveri P., Henahan M. J., Rae J. W. B., Mortyn P. G. and Vance
908 D., Boron isotope evidence for oceanic carbon dioxide leakage during the last deglaciation. *Nature*, 518,
909 219–222, 2015b.
- 910 Martínez-Botí, M. A., Mortyn, P. G., Schmidt, D. N., Vance, D. and Field, D. B., Mg/Ca in foraminifera from
911 plankton tows: Evaluation of proxy controls and comparison with core tops, *Earth Planet. Sci. Lett.*, 307,
912 113–125, 2011.
- 913 Mavromatis, V., Montouillout, V., Noireaux, J., Gaillardet, J. and Schott, J., Characterization of boron
914 incorporation and speciation in calcite and aragonite from co-precipitation experiments under controlled
915 pH, temperature and precipitation rate, *Geochim. Cosmochim. Acta*, 150, 299–313, 2015.

- 916 McCulloch, M. T., D'Olivo, J. P., Falter, J. L., Georgiou, L., Holcomb, M., Montagna, P. and Trotter, J. A.,
 917 Boron Isotopic Systematics in Scleractinian Corals and the Role of pH Up-regulation, *Boron Isot. Adv.*
 918 *Isot. Geochemistry*, 2018.
- 919 Misra, S., Greaves, M., Owen, R., Kerr, J., Elmore, A. C. and Elderfield, H.: Determination of B/Ca of natural
 920 carbonates by HR-ICP-MS, *Geochemistry, Geophys. Geosystems*, 15, 1617–1628, 2014a.
- 921 Misra, S., Owen, R., Kerr, J., Greaves, M. and Elderfield, H., Determination of $\delta^{11}\text{B}$ by HR-ICP-MS from mass
 922 limited samples: Application to natural carbonates and water samples, *Geochim. Cosmochim. Acta*, 140,
 923 531–552, 2014b.
- 924 Mortyn, P. G. and Charles, C. D., Planktonic foraminiferal depth habitat and $\delta^{18}\text{O}$ calibrations: Plankton tow
 925 results from the Atlantic sector of the Southern Ocean, *Paleoceanography*, 18, 2003.
- 926 Mulitza, S., Boltovskoy, D., Donner, B., Meggers, H., Paul, A. and Wefer, G., Temperature: $\delta^{18}\text{O}$ relationships
 927 of planktonic foraminifera collected from surface waters, *Palaeogeogr. Palaeoclimatol. Palaeoecol.*, 202,
 928 143–152, 2003.
- 929 Ni, Y., Foster, G. L., Bailey, T., Elliott, T., Schmidt, D. N., Pearson, P., Haley, B. and Coath, C., A core top
 930 assessment of proxies for the ocean carbonate system in surface-dwelling foraminifers, *Paleoceanography*
 931 22, 2007.
- 932 Nir, O., Vengosh, A., Harkness, J. S., Dwyer, G. S. and Lahav, O., Direct measurement of the boron isotope
 933 fractionation factor: Reducing the uncertainty in reconstructing ocean paleo-pH, *Earth Planet. Sci. Lett.*,
 934 414, 1–5, 2015.
- 935 Noireaux, J., Mavromatis, V., Gaillardet, J., Schott, J., Montouillout, V., Louvat, P., Rollion-Bard, C. and
 936 Neuville, D. R., Crystallographic control on the boron isotope paleo-pH proxy, *Earth Planet. Sci. Lett.*,
 937 430, 398–407, 2015.
- 938 Orr, J. C., Fabry, V. J., Aumont, O., Bopp, L., Doney, S. C., Feely, R. A., Gnanadesikan, A., Gruber, N., Ishida,
 939 A., Joos, F., Key, R. M., Lindsay, K., Maier-Reimer, E., Matear, R., Monfray, P., Mouchet, A., Najjar, R.
 940 G., Plattner, G. K., Rodgers, K. B., Sabine, C. L., Sarmiento, J. L., Schlitzer, R., Slater, R. D., Totterdell, I.
 941 J., Weirig, M. F., Yamanaka, Y. and Yool, A., Anthropogenic ocean acidification over the twenty-first
 942 century and its impact on calcifying organisms, *Nature*, 437, 681–686, 2005.
- 943 Pagani, M., Marked Decline in Atmospheric Carbon Dioxide Concentrations During the Paleogene, *Science*,
 944 309, 600–603, 2005.
- 945 Palmer, M. R., Pearson, P. N. and Cobb, S. J., Reconstructing Past Ocean pH-Depth Profiles, *Science*, 282,
 946 1468–1471, 1998.
- 947 Pearson, P. N. and Palmer, M. R., Middle Eocene seawater pH and atmospheric carbon dioxide concentrations,
 948 *Science*, 284, 1824–1826, 1999.
- 949 Peeters, F. J. C. and Brummer, G.J. a., The seasonal and vertical distribution of living planktic foraminifera in
 950 the NW Arabian Sea, *Geol. Soc. London, Spec. Publ.*, 195, 463–497, 2002.
- 951 Quintana Krupinski, N. B., Russell, A. D., Pak, D. K. and Paytan, A., Core-top calibration of B/Ca in Pacific
 952 Ocean *Neoglobobulimina incompta* and *Globigerina bulloides* as a surface water carbonate system proxy,
 953 *Earth Planet. Sci. Lett.*, 466, 139–151, 2017.
- 954 Rae, J.W.B.: Boron Isotopes in Foraminifera: Systematics, Biomineralisation, and CO₂ Reconstruction. In,
 955 Marschall, H., Foster, G. (eds), *Boron Isotopes. Advances in Isotope Geochemistry*. Springer, Cham, 2018.
- 956 Rae, J. W. B., Foster, G. L., Schmidt, D. N. and Elliott, T., Boron isotopes and B/Ca in benthic foraminifera:
 957 Proxies for the deep ocean carbonate system, *Earth Planet. Sci. Lett.*, 302, 403–413, 2011.

- 958 Raitzsch, M., Bijma, J., Benthien, A., Richter, K.-U., Steinhofel, G. and Kučera, M., Boron isotope-based
 959 seasonal paleo-pH reconstruction for the Southeast Atlantic – A multispecies approach using habitat
 960 preference of planktonic foraminifera, *Earth Planet. Sci. Lett.*, 487, 138–150, 2018.
- 961 Ravelo, A. C. and Fairbanks, R. G., Oxygen isotopic composition of multiple species of planktonic foraminifera:
 962 recorder of the modern photic zone temperature gradient, *Palaeogeogr. Palaeoclimatol. Palaeoecol.*, 7,
 963 815–831, 1992.
- 964 Rebotim, A., Voelker, A. H. L., Jonkers, L., Waniek, J. J., Meggers, H., Schiebel, R., Fraile, I., Schulz, M., and
 965 Kucera, M., Factors controlling the depth habitat of planktonic foraminifera in the subtropical eastern
 966 North Atlantic, *Biogeosciences*, 14, 827–859, <https://doi.org/10.5194/bg-14-827-2017>, 2017.
- 967 Regenberg, M., Steph, S., Nürnberg, D., Tiedemann, R. and Garbe-Schönberg, D.: Calibrating Mg/Ca ratios of
 968 multiple planktonic foraminiferal species with $\delta^{18}\text{O}$ -calcification temperatures, *Paleothermometry for the*
 969 *upper water column*, *Earth Planet. Sci. Lett.*, 278, 324–336, 2009.
- 970 Rickaby, R. E. M. and Halloran, P., Cool La Nina During the Warmth of the Pliocene?, *Science*, 307, 1948–
 971 1952, 2005.
- 972 Ries, J. B., Cohen, A. L. and McCorkle, D. C., Marine calcifiers exhibit mixed responses to CO₂-induced ocean
 973 acidification, *Geology*, 37, 1131–1134, 2009.
- 974 Rink, S., Kühl, M., Bijma, J. and Spero, H. J., Microsensor studies of photosynthesis and respiration in the
 975 symbiotic foraminifer *Orbulina universa*, *Mar. Biol.*, 131, 583–595, 1998.
- 976 Rollion-Bard, C. and Erez, J., Intra-shell boron isotope ratios in the symbiont-bearing benthic foraminiferan
 977 *Amphistegina lobifera*: Implications for $\delta^{11}\text{B}$ vital effects and paleo-pH reconstructions, *Geochim.*
 978 *Cosmochim. Acta*, 74, 1530–1536, 2010.
- 979 Rostek, F., Ruhland, G., Bassinot, F. C., Muller, P. J., Labeyrie, L. D., Lancelot, Y. and Bard, E., Reconstructing
 980 Sea-Surface Temperature and Salinity Using $\delta^{18}\text{O}$ and Alkenone Records, *Nature*, 364, 319–321, 1993.
- 981 Russell, A. D., Hönisch, B., Spero, H. J. and Lea, D. W., Effects of seawater carbonate ion concentration and
 982 temperature on shell U, Mg, and Sr in cultured planktonic foraminifera, *Geochim. Cosmochim. Acta*, 68,
 983 4347–4361, 2004.
- 984 Sanyal, A., Bijma, J., Spero, H. J. and Lea, D. W., Empirical relationship between pH and the boron isotopic
 985 composition of *Globigerinoides sacculifer*: Implications for the boron isotopes paleo-pH proxy,
 986 *Paleoceanography*, 16, 515–519, 2001.
- 987 Sanyal, A., Hemming, N. G., Broecker, W. S., Lea, D. W., Spero, H. J., & Hanson, G. N. Oceanic pH control on
 988 the boron isotopic composition of foraminifera: evidence from culture experiments, *Paleoceanography*,
 989 11(5), 513-517, 1996.
- 990 Shaked, Y. and de Vargas, C., Pelagic photosymbiosis: rDNA assessment of diversity and evolution of
 991 dinoflagellate symbionts and planktonic foraminiferal hosts, *Marine Ecology Progress Serie*, 325, 59–71,
 992 2006.
- 993 Schmidt, G. A. and Mulitza, S., Global calibration of ecological models for planktic foraminifera from core-top
 994 carbonate oxygen-18, *Mar. Micropaleontol.*, 44, 125–140, 2002.
- 995 Seki, O., Foster, G. L., Schmidt, D. N., Mackensen, A., Kawamura, K. and Pancost, R. D., Alkenone and boron-
 996 based Pliocene pCO₂ records, *Earth Planet. Sci. Lett.*, 292, 201–211, 2010.
- 997 Shirayama, Y., Effect of increased atmospheric CO₂ on shallow water marine benthos, *J. Geophys. Res.*, 110,
 998 C09S08, 2005.

- 999 Sime, N. G., De La Rocha, C. L. and Galy, A., Negligible temperature dependence of calcium isotope
1000 fractionation in 12 species of planktonic foraminifera, *Earth Planet. Sci. Lett.*, 232, 51–66, 2005.
- 1001 Spero H. J., Symbiosis in the planktonic foraminifer, *orbulina universa*, and the isolation of its symbiotic
1002 dinoflagellate, *gymnodinium beii* sp.nov, *J. Phycol* 23, 307-317, 1987.
- 1003 Sutton, J. N., Liu, Y. W., Ries, J. B., Guillermic, M., Ponzevera, E. and Eagle, R. A., $\delta^{11}\text{B}$ as monitor of
1004 calcification site pH in divergent marine calcifying organisms, *Biogeosciences*, 15, 1447–1467, 2018.
- 1005 Takagi H., Kimoto K., Fujiki T., Saito H., Schmidt C. and Kucera M., Characterizing photosymbiosis in modern
1006 planktonic foraminifera, *biogeosciences*, 3377–3396, 2019.
- 1007 Thomson, J., Brown, L., Nixon, S., Cook, G. T. and MacKenzie, A. B., Bioturbation and Holocene sediment
1008 accumulation fluxes in the north-east Atlantic Ocean (Benthic Boundary Layer experiment sites), *Mar.*
1009 *Geol.*, 169, 21–39, 2000.
- 1010 Tripathi, A., Deep-Sea Temperature and Circulation Changes at the Paleocene-Eocene Thermal Maximum.
1011 *Science*, 308, 1894–1898, 2005.
- 1012 Tripathi, A. K., Roberts, C. D. and Eagle, R. A., Coupling of CO₂ and Ice Sheet Stability Over Major Climate
1013 Transitions of the Last 20 Million Years, *Science*, 326, 1394–1397, 2009.
- 1014 Tripathi, A. K., Roberts, C. D., Eagle, R. A. and Li, G., A 20 million year record of planktic foraminiferal B/Ca
1015 ratios: Systematics and uncertainties in pCO₂ reconstructions, *Geochim. Cosmochim. Acta*, 75, 2582–
1016 2610, 2011.
- 1017 Uchikawa, J., Penman, D. E., Zachos, J. C. and Zeebe, R. E., Experimental evidence for kinetic effects on B/Ca
1018 in synthetic calcite: Implications for potential B(OH)₄⁻ and B(OH)₃ incorporation, *Geochim. Cosmochim.*
1019 *Acta*, 150, 171–191, 2015.
- 1020 Urey, H.C., Lowenstam, H.A., Epstein, S. & McKinney, C.R.: Measurement of paleo-temperature and
1021 temperatures of the upper cretaceous of England, Denmark, and the southeastern United-States. *Geol. Soc.*
1022 *Am. Bull.*, 62, 399-416, 1951.
- 1023 Wang, B.-S., You, C.-F., Huang, K.-F., Wu, S.-F., Aggarwal, S. K., Chung, C.-H. and Lin, P.-Y., Direct
1024 separation of boron from Na- and Ca-rich matrices by sublimation for stable isotope measurement by MC-
1025 ICP-MS, *Talanta*, 82, 1378–1384, 2010.
- 1026 Wang, G., Cao, W., Yang, D. and Xu, D., Variation in downwelling diffuse attenuation coefficient in the
1027 northern South China Sea, *Chinese J. Oceanol. Limnol.*, 26, 323–333, 2008.
- 1028 Weare, B. C., Strub, P. T. and Samuel, M. D., Annual Mean Surface Heat Fluxes in the Tropical Pacific Ocean,
1029 *J. Phys. Oceanogr.*, 11, 705–717, 1981.
- 1030 Wei, G., McCulloch, M. T., Mortimer, G., Deng, W. and Xie, L., Evidence for ocean acidification in the Great
1031 Barrier Reef of Australia, *Geochim. Cosmochim. Acta*, 73, 2332–2346, 2009.
- 1032 Wilson, D. J., Piotrowski, A. M., Galy, A. and McCave, I. N., A boundary exchange influence on deglacial
1033 neodymium isotope records from the deep western Indian Ocean, *Earth Planet. Sci. Lett.*, 341–344, 35–47,
1034 2012.
- 1035 Wolf-Gladrow, D. A., Riebesell, U., Burkhardt, S. and Buma, J., Direct effects of CO₂ concentration on growth
1036 and isotopic composition of marine plankton, *Tellus B Chem. Phys. Meteorol.*, 51, 461–476, 1999.
- 1037 Yu, J., Menviel, L., Jin, Z. D., Thornalley, D. J. R., Barker, S., Marino, G., Rohling, E. J., Cai, Y., Zhang, F.,
1038 Wang, X., Dai, Y., Chen, P. and Broecker, W. S., Sequestration of carbon in the deep Atlantic during the
1039 last glaciation, *Nat. Geosci.*, 9, 319–324, 2016.

- 1040 Yu, J., Thornalley, D. J. R., Rae, J. W. B. and McCave, N. I., Calibration and application of B/Ca, Cd/Ca, and δ
1041 ^{11}B in *Neogloboquadrina pachyderma* (sinistral) to constrain CO_2 uptake in the subpolar North Atlantic
1042 during the last deglaciation, *Paleoceanography*, 28, 237–252, 2013.
- 1043 Yu, J., Foster, G. L., Elderfield, H., Broecker, W. S. and Clark, E., An evaluation of benthic foraminiferal B/Ca
1044 and $\delta^{11}\text{B}$ for deep ocean carbonate ion and pH reconstructions, *Earth Planet. Sci. Lett.*, 293, 114–120, 20,
1045 2010.
- 1046 Yu, J., Elderfield, H., Hönisch, B., B/Ca in planktonic foraminifera as a proxy for surface seawater pH.
1047 *Paleoceanography* 22, PA2202, 2007.
- 1048 Yu, J., Day, J., Greaves, M. and Elderfield, H., Determination of multiple element/calcium ratios in foraminiferal
1049 calcite by quadrupole ICP-MS, *Geochemistry, Geophys. Geosystems* 6, 2005.
- 1050 Zeebe, R. E. and Wolf-Gladrow, D., *CO₂ in Seawater: Equilibrium, Kinetics, Isotopes* Elsevier Oceanography
1051 Series 65, Amsterdam, 2001.
- 1052 Zeebe, R. E., Wolf-Gladrow, D. A., Bijma, J. and Hönisch, B., Vital effects in foraminifera do not compromise
1053 the use of $\delta^{11}\text{B}$ as a paleo- pH indicator: Evidence from modeling, *Paleoceanography*, 18, 2003.

1054 **Figure caption**

1055
1056 **Figure 1:** (A) Speciation of $B(OH)_3$ and $B(OH)_4^-$ as function of seawater pH (total scale), (B) $\delta^{11}B$ of dissolved
1057 inorganic boron species as a function of seawater pH, (C) sensitivity of $\delta^{11}B$ of $B(OH)_4^-$ for a pH ranging from 7.6
1058 to 8.4. $T=25^\circ C$, $S=35$, $\delta^{11}B=39.61 \text{ ‰}$ (Foster et al., 2010), dissociation constant $\alpha = 1.0272$ (Klochko et al., 2006).

1059
1060 **Figure 2:** Map showing locations of the core-tops used in this study (white diamonds). Red open circles represent
1061 the sites used for *in situ* carbonate parameters from GLODAP database (Key et al., 2004).

1062
1063 **Figure 3:** Pre-industrial data versus depth for the sites used in this study. The figure shows seasonal temperatures
1064 (extracted from World Ocean Database 2013), density anomaly (kg/m^3), pre-industrial pH and pre-industrial $\delta^{11}B$
1065 of $H_4BO_4^-$ (calculated from the GLODAP database and corrected for anthropogenic inputs). Dotted lines are the
1066 calculated uncertainties based on errors on TA and DIC from the GLODAP database.

1067
1068 **Figure 4:** Boron isotopic measurements of mixed-layer foraminifera plotted against $\delta^{11}B_{borate}$. $\delta^{11}B_{borate}$ was
1069 characterized by determination of the calcification depth of foraminifera utilizing data presented in Fig. 3. A) *G.*
1070 *ruber*, B) *T. sacculifer*, C) *O. universa*. Mono-specific calibrations (Table 3) and error bars on $\delta^{11}B_{borate}$ were
1071 derived utilizing the wild bootstrap code from Henehan et al. (2016), while errors on the $\delta^{11}B_{carbonate}$ for this study
1072 are reported as 2σ of measured AE121 standards during the session of the sample. Calibrations were also derived
1073 on the 250-400 size fraction for *G. ruber* and *T. sacculifer* (black dashed lines). Data reported on those graphs
1074 have been measured with an MC-ICP-MS.

1075
1076 **Figure 5:** Boron isotopic measurements of deep-dwelling foraminifera ($\delta^{11}B_{carbonate}$) plotted against $\delta^{11}B_{borate}$.
1077 $\delta^{11}B_{borate}$ was constrained using foraminiferal calcification depths. A) *P. obliquiloculata*, B) *G. menardii*, C) *N.*
1078 *dutertrei*, D) *G. tumida* and E) Compilation of deep dweller species. Mono-specific calibrations are summarized
1079 in Table 3.

1080
1081 **Figure 6:** Boxplots of B/Ca ratios for multiple foraminifera species., including *T. sacculifer* (this study; Foster et
1082 al., 2008; Ni et al; 2007; Seki et al., 2010), *G. ruber* (this study; Babila et al., 2014; Foster et al., 2008; Ni et al.,
1083 2007), *G. inflata*, *G. bulloides* (Yu et al., 2007), *N. pachyderma* (Hendry et al., 2009; Yu et al., 2013), *N. dutertrei*
1084 (this study; Foster et al., 2008), *O. universa*, *P.obliquiloculata*, *G. menardii*, *G. tumida* (this study).

1085
1086 **Figure 7:** A) Boxplot showing the calculated microenvironment pH difference (Δ microenvironment pH) between
1087 microenvironment and external pH based on the $\delta^{11}B$ data. B) This figure shows that a decrease in insolation can
1088 explain the low $\delta^{11}B$ from the WEP. Light penetration profile in the Western Pacific, with E_0 in the WEP of 220
1089 $J.s^{-1}.m^{-2}$ (Weare et al., 1981) and a light attenuation coefficient of $0.028 (m^{-1})$ (Wang et al., 2008). Theoretical
1090 depths were calculated for a decrease in microenvironment pH of $\Delta pH_1 = -0.02$ (e.g. WP07-a); $\Delta pH_1 = -0.04$ (e.g.
1091 A14), $\Delta pH_2 = -0.06$ (e.g. 806A). Light penetration corresponding to E_c is $\sim 12\%$, $\Delta pH_0 \sim 7\%$, $\Delta pH_1 \sim 5\%$, $\Delta pH_2 \sim 1\%$
1092 respective calcification depth are 75m, 90m, 110m and 150m. Grey band is the calcification depth calculated that

1093 explains the Δ microenvironment pH from ΔpH_0 to ΔpH_2 . Dotted lines show the range of the calcification depth
1094 for *T. sacculifer* (w/o sacc) in the WEP utilized in this study.

1095

1096 **Figure 8:** Water depth pH profiles reconstructed at every site applying the mono-specific calibrations derived from
1097 our results (Table 3). Figure is showing measured $\delta^{11}\text{B}_{\text{calcite}}$, $\delta^{11}\text{B}_{\text{borate}}$ calculated according to different calibrations
1098 (see Table 3 and text), calculated pH based on $\delta^{11}\text{B}$ ($\text{pH}_{\delta^{11}\text{B}}$) and pCO_2 calculated from $\text{pH}_{\delta^{11}\text{B}}$ and alkalinity.

1099

1100 **Figure 9:** Evaluation of the reconstructed parameters, $\delta^{11}\text{B}_{\text{borate}}$, pH and pCO_2 versus *in situ* parameter calculated
1101 in Fig. 8 (based on $\delta^{11}\text{B}$ and alkalinity). The recalculated parameters are consistent with *in situ* data, except for *G.*
1102 *rubra*, and this variability might be explained by the different test sizes within measured size fractions.

1103 **Table caption**

1104

1105 **Table 1:** Box-core information

1106

1107 **Table 2:** Analytical results of $\delta^{13}\text{C}$, $\delta^{18}\text{O}$, $\delta^{11}\text{B}$ and elemental ratios Li/Ca, B/Ca and Mg/Ca

1108

1109 **Table 3:** Species-specific $\delta^{11}\text{B}_{\text{carbonate}}$ to $\delta^{11}\text{B}_{\text{borate}}$ calibrations from literature and from our data